Rigorous non-isothermal modeling approach for mass and energy transport during CO2 absorption into aqueous solution of amino acid ionic liquids in hollow fiber membrane contactors

Qazi Sohaib, Amir Muhammad, Mohammad Younas, Mashallah Rezakazemi, Stéphanie Druon-Bocquet, José Sanchez-Marcano

Rigorous Non-Isothermal Modelling Approach for Mass and Energy Transport during CO_2 Absorption into Aqueous Solution of Amino Acid Ionic Liquids in Hollow Fiber Membrane Contactors

Qazi Sohaib[1], Amir Muhammad[2], Mohammad Younas[3], Mashallah Rezakazemi[4,*], Stéphanie Druon-Bocquet[1], José Sanchez-Marcano[1]

1: Institut Européen des Membranes, IEM – UMR 5635, CNRS, ENSCM, Université de Montpellier, Montpellier, France

2: Pak-Austria Fachhochschule: Institute of Applied Sciences &Technology (PAF-IAST), Haripur, Pakistan

3: Department of Chemical Engineering, University of Engineering and Technology, Peshawar, P.O. Box 814, University Campus, Peshawar 25120, Pakistan

4: Faculty of Chemical and Materials Engineering, Shahrood University of Technology, Shahrood, Iran

Corresponding author: mashalah.rezakazemi@gmail.com

Abstract

In the current study, a rigorous modeling approach was used to develop a mathematical model for the non-isothermal absorption process of CO_2 in hollow fiber membrane contactors (HFMC). Four amino acid-based ionic liquids (ILs) namely, tetramethylammonium glycinate $[N_{1111}][Gly]$, 1-ethyl-3-methylimidazolium glycinate $[C_2mim][Gly]$, 1-butyl-3-methylimidazolium glycinate $[C_4mim][Gly]$ and 1-hexyl-3-methylimidazolium glycinate $[C_6mim][Gly]$ were used as absorbents. These ILs have never been implemented for the membrane contactor CO_2 absorption operations both on the lab scale and industrial scale. Wide ranges of operating conditions were investigated for freshly unloaded absorbents and partial conversion of absorbents considering steady-state conditions for the model. Non-wetting conditions were adopted by keeping very low transmembrane pressure. The non-isothermal model predicted a significant temperature rise along the contactor length, ranging from 10-25 K which further affected the absorption and reaction kinetics. Simulations confirmed the strong influence of absorbent concentration and mild influence of process temperature on the separation performance of ILs, CO_2 boundary flux and reaction kinetics between CO_2 and ILs. Very fast absorption of CO_2 near the interface justified the dominancy of the chemisorption for the current absorption. Finally, the comparison with experimental data evidenced the identical trends and hence validated the model.

Keywords: Non-isothermal modelling, CO_2 absorption, Amino acid ionic liquids, Hollow fiber membrane contactor, Chemisorption

1 Introduction

Carbon dioxide (CO_2) gas is one of the major contributors to global warming and climate change. The fossil fuel-based power sectors are the largest sources of CO_2 emissions [1]. Therefore, it is of great importance to implement CO_2 capture technologies in power sectors [1,2]. Post-combustion carbon capture (PCCC) is one of the widely studied technologies for carbon reduction as it holds the greatest advantage of retrofitting to existing units in power plants [3,4]. Some of the main challenges of this process include low flue gas pressure (≈1 atm) and low CO_2 concentration (< 16 %) [5]. However, the liquid absorbent based PCCC is still recognized as state of the art carbon capture technology as it can provide a high CO_2 absorption efficiency (> 80 %) even at low concentrations of CO_2 [3,6].

Currently, amine-based absorbents represent more than 90 % of the market and are regarded as a leading technology for CO_2 capture [7]. Amines are widely used absorbents for CO_2 capture due to their high reactivity with CO_2 and high absorption capacity [8]. However, these absorbents have several drawbacks, including, high corrosion rate, high construction rate, degradation by some gases like SO_2 or NO_2 and high volatility [9–11]. Alternative absorbents have been proposed like ionic liquids (ILs), which can overcome the drawbacks of conventional absorbents [12–14]. Low volatility, negligible vapor pressure, thermal stability, high CO_2 solubility, less toxicity, and low corrosion rates are the main features of ILs [15–19]. These ILs have been divided into two categories, Room temperature ILs (RTILs) and Task-specific ILs (TSILs) or functionalized ILs. RTILs are conventional ILs that provide typical physical solvent behavior for the gas solubility following Henry's Law. Most of the RTILs have very high CO_2 solubility compared to other gases such as N_2, O_2, H_2 and CH_4 [20,21]. TSILs provide very high CO_2 solubility which can reach up to three times of the corresponding alkyl chain RTILs. These ILs are able to absorb CO_2 by both chemical and physical sorption, for which the CO_2 loading increases with an increase in pressure. The

chemical absorption of TSILs can be represented by chemical reaction, while the physical absorption of TSILs can be represented using Henry's law constant. TSILs can absorb CO_2 at low partial pressures due to the chemical reactions [22]. Some of the TSILs developed by researchers for CO_2 capture include protic ILs [23], amino acid-based ILs [24] and amine-based ILs [25,26]. Among these ILs, amino acid-based ILs got more attention recently because of their high CO_2 capacity and high solubility in water [27].

Differential gas-liquid contactors (packed columns, bubble columns and spray towers) and stage-wise gas-liquid contactors (plate columns and rotating disc contactors) are currently used absorbers on an industrial scale. Liquid holdup and gas-liquid interfacial area are the important parameters in the design of this equipment [28]. The above-mentioned absorbers face some crucial problems including high energy consumption, flooding, foaming, solvent loss due to degradation and entrainments, equipment corrosion and large footprint. Hollow fiber membrane contactor (HFMC) technology is an alternative to overcome these problems [29–33]. Membrane contactors are non-dispersive contacting systems in which the membrane does not provide selectivity by itself and rather works as a barrier between gas and liquid and increases the mass transfer area. The advantages of the membrane contactor include non-dispersive mass transfer operations, high known and constant interfacial area, operational flexibility and modularity [28,34–36]. Falk-Pedersen et al. [36] used aqueous solution (30 wt.%) of mono-ethanolamine (MEA) in a membrane contactor for the absorption of exhaust gases from a gas turbine on an offshore installation. Serval benefits have been reported including 38-42 % savings of operating cost, 35-40 % capital cost reduction, 34-40 % equipment weight reduction and 40-50% footprint requirement reduction. Chabanon et al. [37] studied the process intensification of membrane contactor setup with concentrated MEA solutions. The maximum intensification factor was obtained with 70 wt.% MEA concentration at 60 ^{o}C. Lu et al. [38] developed a membrane contactor CO_2 absorption setup using aqueous

mixture of 2-amino-2-methyl-1-propanol (AMP) and ILs 1-butyl-3-methyl-imidazolium tetrafluoroborate [bmim][BF4] and 1-(3-aminopropyl)-3-methyl-imidazolium tetrafluoroborate [apmim][BF4]. The setup was investigated for the cyclic and non-cyclic absorption process, static regeneration process and continuous absorption and regeneration process. The blended (AMP and IL) absorbents were able to achieve higher net and circular absorption capacities compared to the pure IL in the coupling process. To overcome the mass transfer limitations of the CO_2 capture process, various technologies were implemented, including supported ILs and encapsulated ILs. The dual functionality (both ILs and support) of the supported ILs enhances the CO_2 capture process [39]. Recently, Sánchez Fuentes et al. [40] developed supported ionic liquid membranes (SILMs) based on three TSILs 1-(2-aminoethyl)-3-methylimidazolium trifluoromethanesulfonate ([AEMIm]Tf), 1-(2-aminoethyl)-3-methylimidazolium tetrafluoroborate ([AEMIm]BF_4) and trioctylmethylammonium anthranilate ([TOMA]), for CO_2/N_2 separation. The SILMs showed very high permselectivity of up to 70. In another work, Zhang et al. [41] developed four diamine-monocarboxylate-based protic ILs for CO_2/N_2 and CO_2/CH_4 separation. A very high selectivity of 151 was reported for CO_2/N_2. Encapsulation of ILs within a porous material increases the effective mass transfer area for CO_2 absorption and reduces the mass transfer resistance[42]. Recently, Santiago et al. [43] encapsulated amino acid based ILs in porous carbon capsules. The author investigated reaction enthalpies and both physical and chemical CO_2 absorption for all ILs. In another study, Romanos et al. [44] developed novel supported IL phase system by encapsulating amine-functionalized ILs within an envelope of silica nanoparticles. The author reported promising CO_2/N_2 separation performance and very fast absorption kinetics.

In the current study four amino-based TSILs tetramethylammonium glycinate [N_{1111}][Gly], 1-ethyl-3-methylimidazolium glycinate [C_2mim][Gly], 1-butyl-3-methylimidazolium glycinate

[C_4mim][Gly] and 1-hexyl-3-methylimidazolium glycinate [C_6mim][Gly] have been investigated for CO_2 capture in a membrane contactor. These ILs have similar anion ([Gly]) and different cations, as shown in Figure 1.

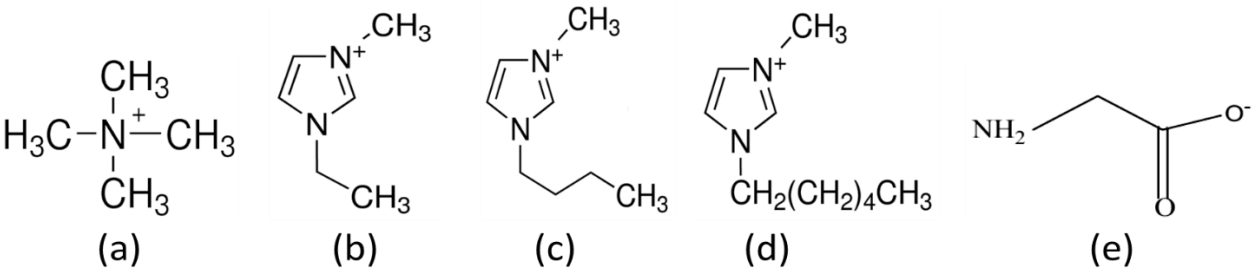

Figure 1. Cations and anion of the ILs (a) $[N_{1111}]^+$, (b) $[C_2mim]^+$, (c) $[C_4mim]^+$, (d) $[C_6mim]^+$ and (e) $[Gly]^-$.

The main drawback of the amino acid-based ILs is their very high viscosities (> 200 mPa.s) which also reduces the diffusivity of CO_2 and slows down the absorption process [45,46]. As these ILs are highly soluble in water, using the aqueous solutions instead of pure ILs can reduce the viscosity to a very low value. The lower viscosities of these aqueous solutions mitigate the flow and pressure drop related problems in the membrane contactors and also enhances CO_2 diffusivitiy [3]. The aqueous solutions of these ILs can provide high surface tension and a very high contact angle with hydrophobic membranes (used in this study), avoiding pore wetting of the membrane. Moreover, these ILs are very highly reactive providing remarkably high solubilities for CO_2 following both chemisorption and physisorption. The above-mentioned properties of these ILs and their aqueous solutions makes them potential candidates for using with hydrophobic membranes.

For this work, the considered ILs are new to the membrane contactor absorption. Up to the authors knowledge, these ILs have never been studied (experimentally as well as modeling) for membrane contactor based CO_2 absorption operations. Most of the models developed for the CO_2 absorption in membrane contactors are based on isothermal behavior. In fact, the process is non-isothermal as the energy of dissolution reaction is released and accumulated along the membrane contactor length, particularly for very reactive absorbents as considered for the current study. Thus, the non-isothermal model developed here provides more realistic approach towards the process of CO_2 absorption in reactive absorbents. The isothermal approach developed in the other studies underestimates the process due to not considering the actual absorption process which is non-isothermal. The current model considers a new approach for the non-isothermal behavior of the chemisorption of CO_2 in the amino acid-based reactive ILs used as absorbents in the membrane contactor. Water evaporation and condensation have been neglected by maintaining the liquid side pressure and introducing a dry gas mixture at the inlet. The steady-state model was implemented to investigate various operating conditions for dry gas mixture, unloaded absorbents and partial conversion of absorbents. The model was able to investigate the non-isothermal behavior of the absorption process and its influence on the axial profiles of reaction and absorption kinetics. Simulations were performed to study the influence of absorbent concentration and process temperature on the separation performance of ILs, CO_2 boundary flux and reaction kinetics between CO_2 and ILs. Moreover, experimental data of CO_2 absorption in membrane contactor were presented and compared with the current simulations.

2 Studied experimental setup and modeling system characteristics

A membrane contactor gas absorption setup suitable for post-combustion CO_2 capture was adopted to be modeled here. A typycal HFMC based post-combustion CO_2 capture setup with liquid on lumen side is presented in Figure 2. The setup has been described by many

reserchers in their studies [37,47–50], and is very suitable especially for industrial applications [3]. Liquid absorbents flows through the tube side of the membrane contactor. Gas streams of N_2 and CO_2 are measured by gas flowmeter for introducing a known concentration of post-combustion gas mixture and to control gas flowrate. Gas streams are introduced to a buffer tank first, to uniformly mix the gases. The mixed gas stream is then allowed to flow countercurrently through the shell side of the membrane contactor. CO_2 from the gas stream is absorbed in the IL whose concentration is monitored with a CO_2 analyzer on the gas side outlet of the memberane contactor. To prevent penetration of gas bubbles to the liquid side, liquid side pressure is always kept slightly higher than the gas side.

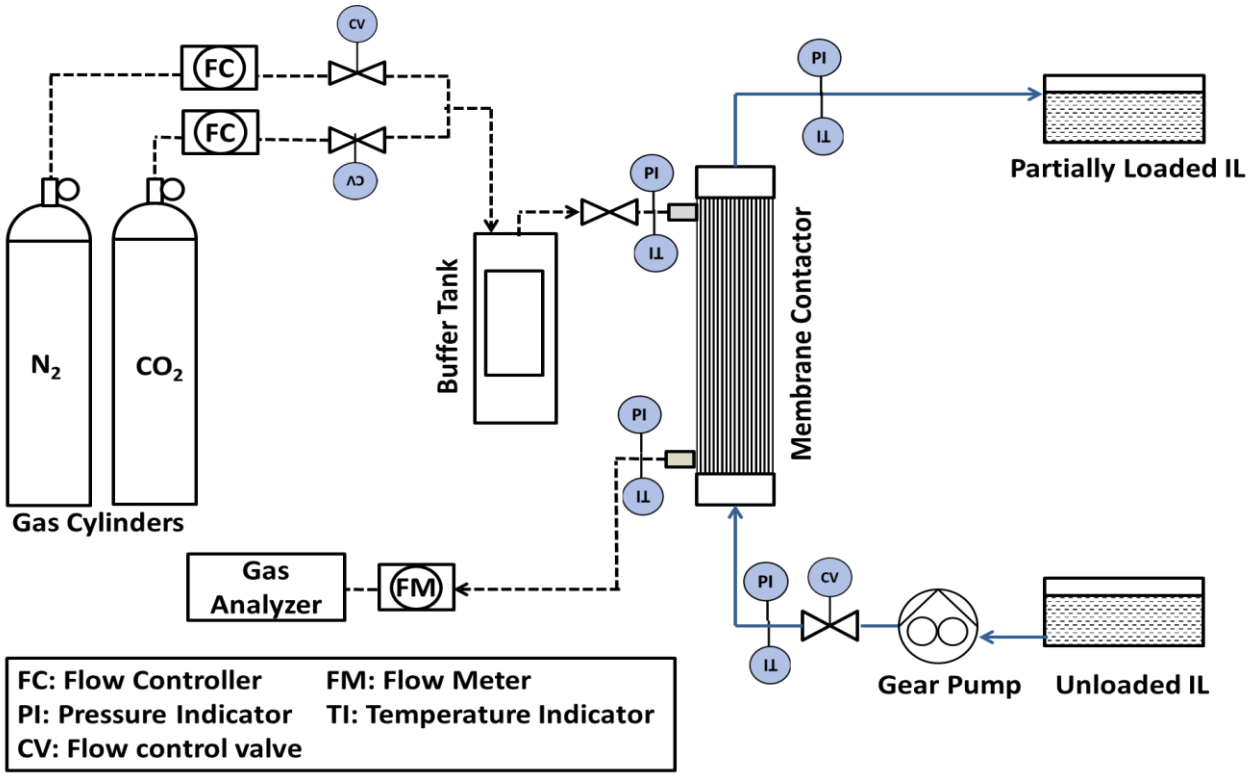

Figure 2. Studied experimental setup; black dashed lines represent gas flow, solid blue lines represent IL flow.

The simplified form of the modeling setup is presented in Figure 3. A microporous hydrophobic membrane contactor (poly-propylene fibers) of parallel configuration was

selected for the study whose characteristics, process parameters and operating conditions are presented in Table 1. Four amino acid-functionalized ILs were also selected as absorbents. The ILs selected were tetramethylammonium glycinate [N_{1111}][Gly] as amino acid-based IL and three imidazolium amino acid ILs namely 1-ethyl-3-methylimidazolium glycinate [C_2mim][Gly], 1-butyl-3-methylimidazolium glycinate [C_4mim][Gly] and 1-hexyl-3-methylimidazolium glycine [C_6mim][Gly]. Dry gas mixture (CO_2+N_2) and absorbents were considered flowing counter currently on the shell side and lumen side of the membrane contactor, respectively. For industrial operations, the reported CO_2 concentration is about 8-15% [51]. Thus, 15% CO_2 concentration is considered throughout the model. The absorption species (CO_2) transfer from the shell side (by convection and diffusion) to the pores of the membrane (only diffusion in the pores) and then absorbs (chemisorption followed by physisorption) in the absorbent on the lumen side of the membrane contactor.

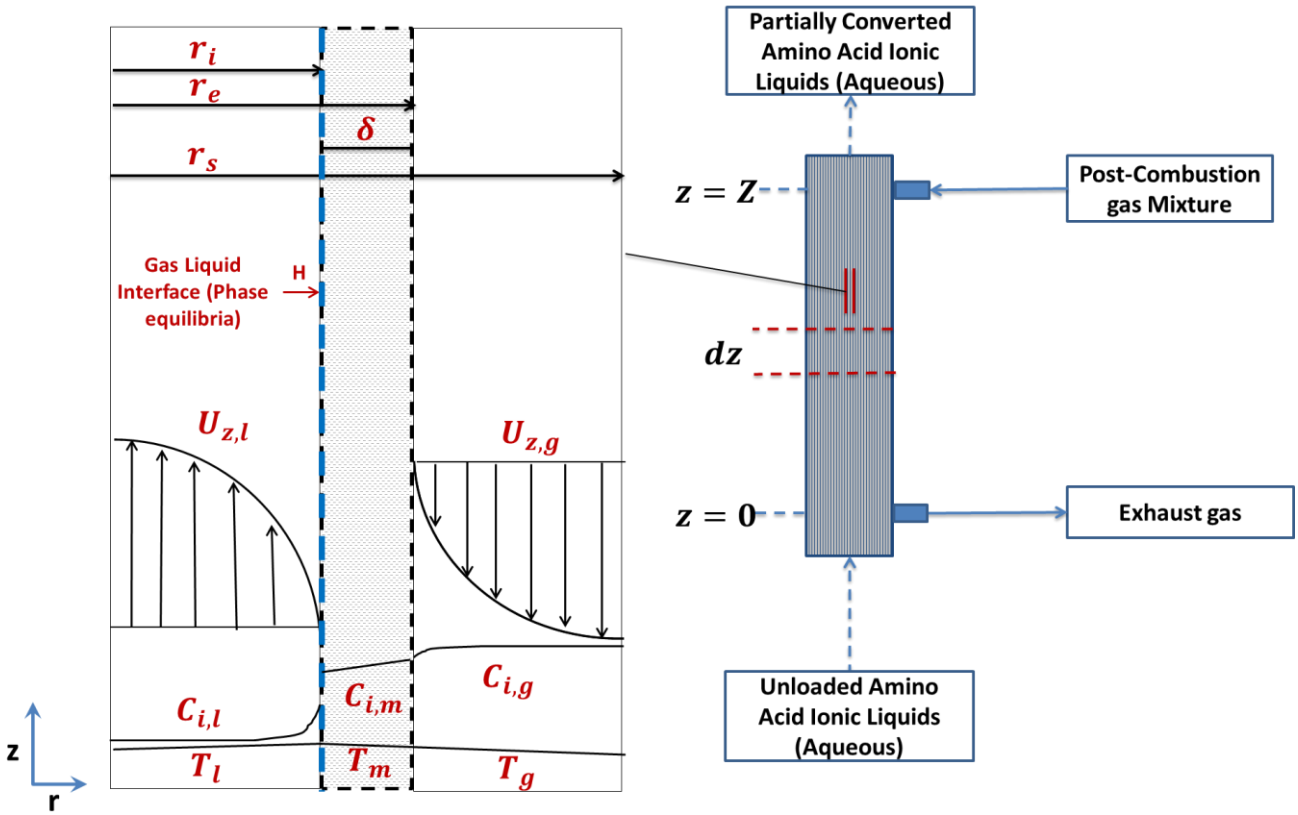

Figure 3 Schematic representation of the membrane contactor PCCC setup and the section used for model development

Table 1 Characteristics of HFMC and operating conditions considered for simulations

Parameter	Value	Unit
HFMC (Hydrophobic, Parallel flow)		
Fiber inner radius (r_i)	2.0×10^{-4}	m
Fiber outer radius (r_e)	2.5×10^{-4}	m
Fiber thickness (δ)	0.5×10^{-4}	m
Fiber length (Z)	0.150	m
Number of fibers (n)	140	-
Porosity (ε)	60	%
Packing factor (∅)	0.30	-
Shell side (gas)		
CO_2 molar fraction	15	%
Flow rate (Q_g)	60	ml min^{-1}
Inlet temperature (T)	298-323	K
Shell side Pressure (P)	2.20	Bar
Lumen side (liquid)		
Absorbent Concentration (C_{IL})	0.3-2	$mol.L^{-1}$
Inlet CO_2 loading of Absorbent (α)	0	$mol.mol^{-1}$
Flow rate(Q_{IL})	20	$ml.min^{-1}$
Inlet temperature (T)	298-323	K
Lumen side Pressure (P)	3.10	Bar

3 Modeling approach

3.1 Model assumptions

A two dimensional (2D) convective and diffusive mass and heat transport model was developed for the ILs based membrane contactor CO_2 capture process presented in Figure 1. The model is based on the non-isothermal absorption process across the membrane contactor. CO_2 is considered to be the only species that can cross the gas-liquid interface. The following assumptions were made to solve the model.

Hydrodynamics:

a) Steady-state conditions
b) Countercurrent arrangements for gas and IL flow in membrane contactor
c) Gas and liquid flow under laminar conditions with fully developed velocity profile with no radial components

Thermodynamics:

a) Application of Henry's law for gas-liquid equilibrium on the interface
b) The membrane works as a non-selective barrier
c) Neglected solubility of N_2
d) Ideal gas behavior

Kinetics, mass transfer, and heat transfer

a) Reversible reaction kinetics
b) Application of Fick's diffusion through porous media for membrane mass transfer, neglecting convective contributions
c) Contributions of advection and diffusion to mass balance solved by considering local concentrations and contributions of convection, conduction, and heat of reaction to energy balance solved by local temperatures.
d) The gas mixture is considered to be dry (no water vapors)
e) Neglecting the presence of water evaporation and condensation

3.2 Model equations

The following continuity equation is considered for the mass balance over the three domains.

$$\frac{\partial C_i}{\partial t} = -\nabla . C_i U - \nabla . j_i + \acute{r}_i \quad (1)$$

Equation (1) in the steady-state form can be written as:

$$0 = -\nabla . C_i U - \nabla . j_i + \acute{r}_i \quad (2)$$

Based on the above-mentioned assumptions, the steady-state continuity equation (2) for the gas, membrane and liquid side are presented below.

$$D_{i,g}\left[\frac{\partial^2 C_{i,g}}{\partial r^2} + \frac{1}{r}\frac{\partial C_{i,g}}{\partial r} + \frac{\partial^2 C_{i,g}}{\partial z^2}\right] = U_{z,g}\frac{\partial C_{i,g}}{\partial z} \quad (3)$$

$$D_{i,m}\left[\frac{\partial^2 C_{i,m}}{\partial r^2} + \frac{1}{r}\frac{\partial C_{i,m}}{\partial r} + \frac{\partial^2 C_{i,m}}{\partial z^2}\right] = 0 \quad (4)$$

$$D_{i,l}\left[\frac{\partial^2 C_{i,l}}{\partial r^2} + \frac{1}{r}\frac{\partial C_{i,l}}{\partial r} + \frac{\partial^2 C_{i,l}}{\partial z^2}\right] + \acute{r}_i = U_{z,l}\frac{\partial C_{i,l}}{\partial z} \quad (5)$$

The thermal balances based on the above-mentioned assumptions are presented below.

$$\lambda_g\left[\frac{\partial^2 T_g}{\partial r^2} + \frac{1}{r}\frac{\partial T_g}{\partial r} + \frac{\partial^2 T_g}{\partial z^2}\right] = U_{z,g}C_{p,g}\rho_g\frac{\partial T_g}{\partial z} \quad (6)$$

$$\lambda_{m,e}\left[\frac{\partial^2 T_m}{\partial r^2} + \frac{1}{r}\frac{\partial T_m}{\partial r} + \frac{\partial^2 T_m}{\partial z^2}\right] = 0\ ; \quad \lambda_{m,e} = \varepsilon\lambda_g + (1-\varepsilon)\lambda_m \quad (7)$$

$$\lambda_l\left[\frac{\partial^2 T_l}{\partial r^2} + \frac{1}{r}\frac{\partial T_l}{\partial r} + \frac{\partial^2 T_l}{\partial z^2}\right] + \acute{r}_i\Delta H_{abs} = U_{z,l}C_{p,l}\rho_l\frac{\partial T_l}{\partial z} \quad (8)$$

Hagen-Poiseuille equation with no-slip conditions was used for the fully developed velocity profile of the fluid on the lumen, while for the shell side Happel's free surface model was used [52].

$$U_{z,g} = 2u_g\left[1 - \left(\frac{r}{r_i}\right)^2\right] \quad (9)$$

$$U_{z,l} = 2u_l\left[1 - (\frac{r_e}{r_s})^2\right]\frac{(r/r_s)^2 - (r_e/r_s)^2 + 2\ln(r_e/r)}{3 + (r_e/r_s)^4 - 4(r_e/r_s)^2 + 4ln(r_e/r_s)}, \quad r_s = r_e\sqrt{\frac{1}{1-\emptyset}}, \quad 1 - \emptyset = \frac{Nr_e^2}{{r_c}^2} \quad (10)$$

3.3 Reaction and absorption kinetics

The four ILs selected for the current study, [N_{1111}][Gly], [C_2mim][Gly], [C_4mim][Gly] and [C_6mim][Gly] have the same glycine ([Gly]) anion and different cations. The mechanism is

similar for the above-mentioned amino acid-based ILs. Glycine based aqueous alkaline salts show similar reactivity for CO_2 as of primary alkanolamines [51,53,54]. The zwitterion mechanism proposed by Caplow [55] for primary alkanol amines is considered as a reaction mechanism for amino acid-based ILs here. CO_2 reacts with the amino acid-based ILs via the formation of zwitterion due to the deprotonation by a base present in the aqueous solution [51].

$$H_2N-CH_2-COO^-R^+ + CO_2 \rightleftharpoons_{K_1}^{K_2} {}^-OOC^+H_2N-CH_2-COO^-R^+ \quad (11)$$

$$^-OOC^+H_2N-CH_2-COO^-R^+ + B_i \rightarrow^{K_{B_i}-} OOCHN-CH_2-COO^-R^+ + B_iH^+ \quad (12)$$

B_i is the base present in the solution to deprotonate zwitterions. Liquid phase equilibrium reactions are as under.

$$^-OOCHN-CH_2-COO^-R^+ + H_2O \rightleftharpoons H_2N-CH_2-COO^-R^+ + HCO_3^- \quad (13)$$

$$H_3N-CH_2-COO^-R^+ \rightleftharpoons H_2N-CH_2-COO^-R^+ + H^+ \quad (14)$$

$$CO_2 + H_2O \rightleftharpoons H^+ + HCO_3^- \quad (15)$$

$$HCO_3^- \rightleftharpoons H^+ + CO_3^- \quad (16)$$

$$H_2O \rightleftharpoons H^+ + OH^- \quad (17)$$

The criterion to determine whether the reaction completely occurs in the bulk or in the liquid film is based on the Hatta number. Hatta number can be defined as under.

$$H_a = \frac{\sqrt{D_i K_{ov}}}{K_l} \quad (18)$$

Where K_{ov} and K_l represent the overall reaction rate constant (s^{-1}) and liquid film mass transfer coefficient (m s^{-1}). To confirm the fast pseudo-first-order regime, the Hatta number must follow the criterion of $2 < H_a \ll E_\infty$ [51,56]. E_∞ represents infinite enhancement factor. When this criterion is fulfilled, the reaction of CO_2 and amino acid based ILs can be considered as in the fast pseudo first order regime which means that change in the

concentration of the absorbent is negligible and reaction is of the first order for CO_2 [57]. ILs $[N_{1111}][Gly]$ [51], $[C_2mim][Gly]$ [54], $[C_4mim][Gly]$ [58] and $[C_6mim][Gly]$ [59] fulfill the criteria of fast pseudo-first-order reaction regime for a range of concentrations. Enhancement factors, Hatta numbers, and second-order rate constants are presented in Table 2. The second-order reaction rate was temperature-dependent and increased with an increase in temperature. The kinetic data for all four ILs (at 1M Concentration) were calculated from the Arrhenius plot and are presented in Table 2.

Table 2 Enhancement factor (E), Hatta number (H_a) and rate constant (K_2) for the ILs

IL concentration (mole L^{-1})	**E 303 K**	**H_a 303 K**	**K_2 (L mol^{-1} s^{-1}) 303 K**	**K_2 (L mol^{-1} s^{-1})**	**Reference**
$[N_{1111}][Gly]$					
0.3	14.56	14.56	242.16	-	[51]
0.7	34.39	34.39	719.34	-	[51]
1.0	41.33	41.33	736.93	4.6930×10^5 exp (-1856/T)	[51]
2.0	62.68	62.68	1297.13	-	[51]
$[C_2mim][Gly]$					
0.5	23.67	23.67	296.29	-	[54]
1.0	51.58	51.58	662.95	6.041×10^6 exp (-2801/T)	[54]
1.5	87.57	87.57	1213.52	-	[54]
2.0	107.15	107.15	1280.78	-	[54]
$[C_4mim][Gly]$					
0.5	28.31	28.31	417.52	-	[58]
1.0	52.65	52.65	675.51	1.3460×10^{10} exp (-5038/T)	[58]
1.5	102.27	102.27	1539.38	-	[58]
2.0	139.49	139.49	1955.60	-	[58]
$[C_6mim][Gly]$					
0.5	36.02	36.02	759.22	-	[59]
0.8	48.86	48.86	1091.81	-	[59]

1.0	57.50	57.50	1402.38	3.04×10^7 exp (-3050/T)	[59]
1.2	66.75	66.75	1855.99	-	[59]

3.4 Solubility, phase equilibria, and diffusion coefficients

The interfacial phase equilibrium for the absorption species was defined as follows.

$$C_{i,l} = m\, C_{i,g} \tag{19}$$

Where m is the dimensionless distribution coefficient for the absorption species which can be presented as below.

$$m = RTH \tag{20}$$

where H represents the solubility of the absorption species. The solubility of CO_2 in IL $[N_{1111}][Gly]$ was estimated by Jing et al. [51] using the Schumpe model [60,61] presented below.

$$\log\left(\frac{H_{i,w}}{H_i}\right) = \sum\left(h_i + h_g\right)C_i \tag{21}$$

Where h_i and h_g represent ion and gas specific constants, respectively and C_i is ion concentration. The solubility of CO_2 in water was calculated as under [62].

$$H_{i,w} = 3.54\ 10^{-7} \exp\left(\frac{2044}{T}\right) \tag{22}$$

The solubility of $[C_2mim][Gly]$, $[C_4mim][Gly]$ and $[C_6mim][Gly]$ was calculated according to the regular solution theory. For ILs the Henry law constant $H^*(atm)$ decreases with an increase in solubility. The regular solution theory is presented below.

$$\ln H^* = a + \frac{b(\delta_1 - \delta_2)^2}{T} \tag{23}$$

Where $\delta(Jcm^{-3})^{\frac{1}{2}}$ represents the solubility parameter, while $a\ (Jcm^{-3})^{-1}$ and $b(Jcm^{-3})^{-1}$ are constants depending on the gas [63,64].

The solubility of CO_2, $H(mol\ m^{-3}Pa^{-1})$ in aqueous solutions of [C₆mim][Gly], [C_2mim][Gly] and [C_4mim][Gly] was found from the Henry law using the parameter H^* [65].

$$H = \frac{10\ \rho}{M\ H^*} \tag{24}$$

Diffusivity of CO_2 and N_2 in the gas phase can be found using the correlation developed by Fuller et al. [66].

$$D_{i,g} = \frac{0.01013\ T^{1.75}\left(\frac{1}{M_{CO_2}}+\frac{1}{M_{N_2}}\right)^{0.5}}{P\left[\left(\sum \upsilon_{CO_2}\right)^{\frac{1}{3}}+\left(\sum \upsilon_{N_2}\right)^{\frac{1}{3}}\right]^2} \tag{25}$$

Diffusivity if CO_2 in the membrane can be calculated from the following equation. The membrane was considered as gas-filled and no wetting conditions were implemented here.

$$\frac{1}{D_{i,m}} = \left[\frac{1}{D_{i,g}} + \frac{1}{D_{Kn}}\right] \tag{26}$$

Where D_{Kn} is the Knudsen diffusion coefficient, which can be found as below.

$$D_{Kn} = \frac{1}{2} d_p \sqrt{\frac{8RT}{\pi M}} \tag{27}$$

where d_p is the membrane pore diameter. The aqueous solutions of [N_{1111}][Gly], [C_2mim][Gly], [C_4mim][Gly] and [C₆mim][Gly] are electrolyte solutions. Equations developed by Barret [67] and Danckwerts [56] were used to calculate the diffusivities of CO_2 in these solutions.

$$\left(D_{i,l}\ {\mu_l}^{0.8}\right)_T = \left(D_{i,w}\ {\mu_w}^{0.8}\right)_T \tag{28}$$

$$\log D_{i,w} = -8.1764 + \frac{712.5}{T} - \frac{2.591\ 10^5}{T^2} \tag{29}$$

3.5 Meshing domains, boundary conditions, and numerical resolution

Meshing and proper discretization of the geometry are very important for the finite element analysis. The current absorption process is mostly controlled by the liquid side resistance. Therefore, a rigorous absorption model with sufficient discretization is needed. Moreover, interfacial chemical reactions were considered in the current absorption process, as it can also be confirmed from the analysis in Section 2.2.3 and the high values of Hatta number presented in Table 2. Refined mapped (rectangular shaped) meshing was implemented across the symmetrical geometry with more refining along with the interface and inside the membrane. The meshed surface along with the labeled boundary conditions (BCs) is presented in Figure 4. BCs for both mass and energy transport equations are presented in Table 3.

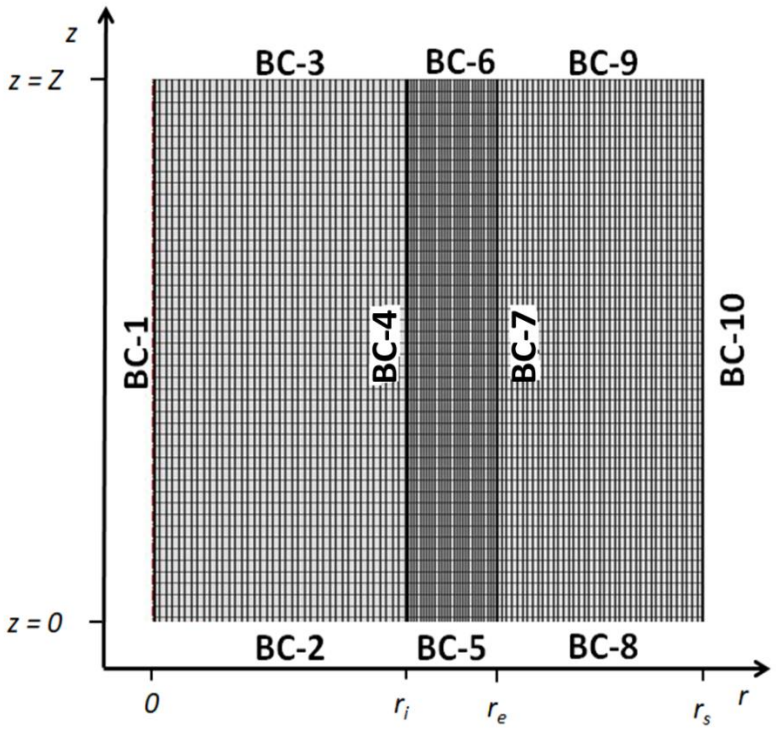

Figure 4 Meshed domains and boundaries of membrane contactor for mass and energy transport

Table 3 Boundary conditions for mass and energy transport

Boundary	Condition	Mass transport	Energy transport

$\boldsymbol{BC-1}$	Axial symmetry	$\frac{\partial C_{i,l}}{\partial r}=0$	$\frac{\partial T_l}{\partial r}=0$
$\boldsymbol{BC-2}$	Inlet liquid conditions	$C_{i,l}=C_{i,l-in}$	$T_l=T_{l-in}$
$\boldsymbol{BC-3}$	Convective flux at liquid outlet	$-D_{i,l}\frac{\partial C_{i,l}}{\partial z}=0$	$-\lambda_l\frac{\partial T_l}{\partial z}=0$
$\boldsymbol{BC-4}$	Interfacial gas liquid equilibrium	$C_{i,l}=mC_{i,m}$	$T_l=T_m$
$\boldsymbol{BC-5}$	No Flux	$-D_{i,m}\frac{\partial C_{i,m}}{\partial z}=0$	$\frac{\partial T_m}{\partial z}=0$
$\boldsymbol{BC-6}$	No Flux	$-D_{i,m}\frac{\partial C_{i,m}}{\partial z}=0$	$\frac{\partial T_m}{\partial z}=0$
$\boldsymbol{BC-7}$	Interfacial continuity	$C_{i,m}=C_{i,g}$	$T_m=T_g$
$\boldsymbol{BC-8}$	Convective flux at gas outlet	$-D_{i,g}\frac{\partial C_{i,g}}{\partial z}=0$	$-\lambda_g\frac{\partial T_g}{\partial z}=0$
$\boldsymbol{BC-9}$	Inlet gas conditions	$C_{i,g}=C_{i,g-in}$	$T_g=T_{g-in}$
$\boldsymbol{BC-10}$	Axial symmetry	$\frac{\partial C_{i,g}}{\partial r}=0$	$\frac{\partial T_g}{\partial r}=0$

The set of 2D model equations presented in the preceding sections are boundary value problems of the partial differential equation system. The model was developed and solved using COMSOL Multiphysics® which uses the finite element method. The solved model was post-processed in MATLAB® and Microsoft Excel.

4 Results and discussion

4.1 Comparison between simulations and experimental data

To validate the model comparison between simulations and experimental data was carried out. Up to the authors knowledge, the ILs used in the current study have never been implemented in the membrane contactor absorption operations. Thus there is no experimental data available in the literature for the ILs considered in this study. Therefore experimental data of the membrane contactor absorption with IL monoethanolamine glycinate ([MEA][Gly]) was used for the comparison with the current simulations. This IL has the same anion, and almost

comparable physicochemical properties as of the ILs used in the simulations here. The experimental setup was adopted from the work of Lu et al. [68] in which IL [MEA][Gly] was used for CO_2 absorption in membrane contactor. Characteristics of the membrane and operating conditions were adopted from Tables 1 and 2, respectively, of their studies. Simulation were performed for the unloaded solvent $C_{i,l\text{-}in}$=0 at temperature T=289 K, gas side pressure P= 1.08 bar, IL concentration C_{IL}= 0.5 mol L^{-1} and gas flow rate Q_g= 800 ml min^{-1}. The liquid flowrate was varied from 80 to 160 ml min^{-1}, and the normalized CO_2 concentration at the gas side outlet was recorded and reported in Figure 5. The square dots represent the experimental data of the IL [MEA][Gly] while the lines represent simulations of the four IL. The relative standard deviations between experimental data points and simulations are very low and are in the range of 1.8 % - 4.1 %. The highest relative standard deviation of 4.1 % was recorded at Q_{IL}= 100 ml min^{-1}, while lowest of 1.8 % was recorded at Q_{IL}= 80 ml min^{-1}. The model seems to be able to closely represent the experimental data. The trends between the experimental data and simulations are identical. Experimental data of [MEA][Gly] shows high separation performance than the simulated ILs, except for the IL [C_6mim][Gly] where the difference in the separation performance is very low. The difference in the separation performance is due to the different physicochemical properties and reactivity of the ILs.

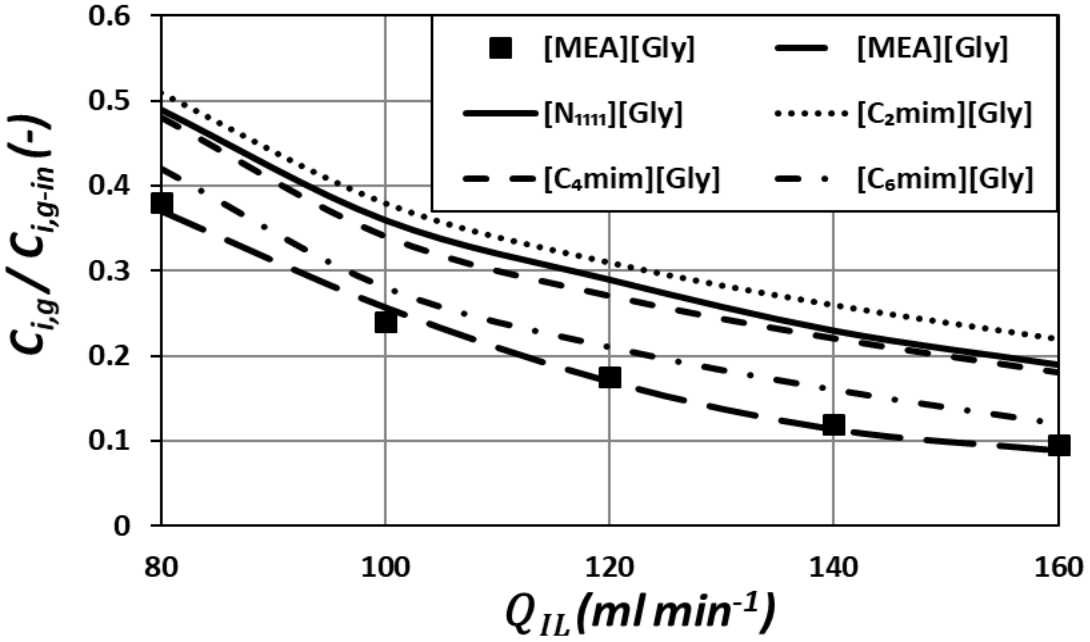

Figure 5 Comparison between the simulations (line) and experimental data (square dots); $Q_g = 800\ ml\ min^{-1}$, $C_{i,l-in} = 0\ mol\ L^{-1}$, $C_{IL-in} = 0.5\ mol\ L^{-1}$, $T_{l-in}, T_{g-in} = 289\ K$

4.2 Axial interfacial profiles: CO_2 concentration, IL concentration, temperature distribution, reaction rate K_2 rise

This section presents the simulations of CO_2 concentration, IL concentration, and variations of temperature and reaction rate constant over the interfacial boundary of the membrane. As mentioned in the preceding sections, the gas/liquid equilibrium over the interfacial boundary is defined by Henry's Law. Hatta numbers presented in Table 2 have confirmed the reaction for absorption species and ILs to occur at the interface mostly. This number can define whether the reaction occurs in the bulk or the liquid film depending upon its value [57]. The steady-state gradual evolution of the axial concentration of CO_2 and IL is presented in Figure 6. Unloaded absorbent was introduced to the tube side at z=0 while the gas mixture having 15 % CO_2 and N_2 (rest to balance) was passed counter currently from the shell side of the membrane contactor. The absorbents were considered to be at chemical equilibrium having homogenous concentration at the inlet of the contactor. A gradual decrease in the

concentrations of both gas-phase CO_2 and absorbent can be observed toward the respective outlets due to absorption at the interface. At the inlet of the gas side, a faster drop in the concentration of CO_2 can be observed which demonstrates the effect of CO_2 concentration on the absorption process. The gradual decrease in the concentration of absorbent along with the fiber length shows the enrichment of the absorbent with CO_2. A similar trend of absorption can be seen for all ILs. ILs $[N_{1111}][Gly]$ and $[C_4mim][Gly]$ have nearly the same concentration profiles. IL $[C_6mim][Gly]$ can be regarded as the most efficient one while $[C_2mim][Gly]$ as the least efficient one among all ILs.

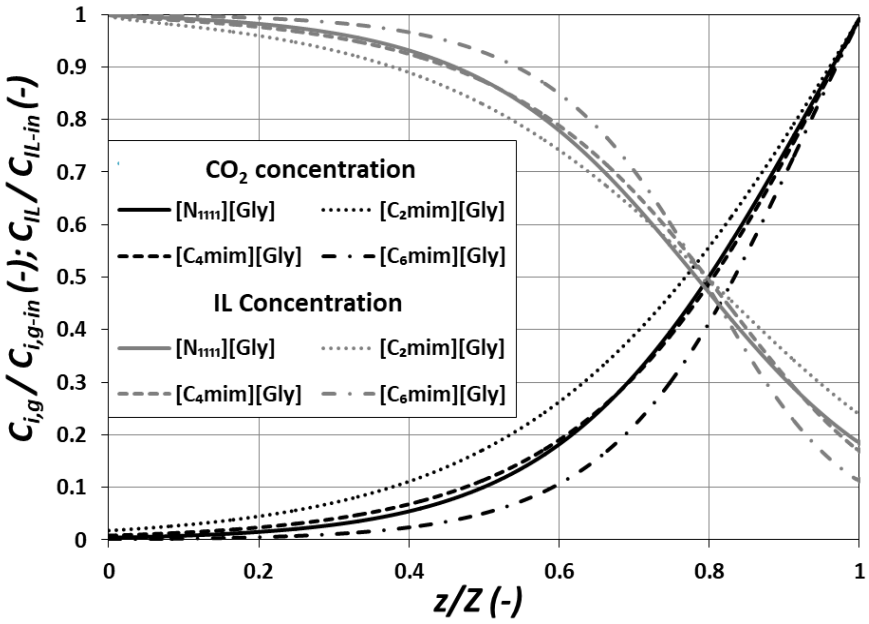

Figure 6 Normalized axial concentration distribution of absorption species (CO_2) and absorbents over mass transfer interface; $Q_{IL} = 20\ ml\ min^{-1}$, $Q_g = 60\ ml\ min^{-1}$, $C_{i,l-in} = 0\ mol\ L^{-1}$, $C_{IL-in} = 1\ mol\ L^{-1}$, $T_{l-in}, T_{g-in} = 298\ K$

Figure 7 shows the axial temperature profile of the liquid phase for the four ILs having an inlet temperature of 298 K. The temperature was recorded near the interface. As mentioned in the assumptions the gas mixture was considered to be dry which helps to avoid the condensation of water vapors near the liquid inlet. The pressure was kept higher to avoid the evaporation of water in the lateral sections near the liquid outlet. The temperature rise ranges

from 10-25 K. The rising of temperature for different ILs can be related to its specific heat and release of energy of dissolution reaction. The temperature rise over the mass transfer interface, where there is a strong chemical reaction, is mostly dependent on the enthalpy of reaction as it is the main heat source. As the reaction occurs over the interface and the reactants move along the fiber length, the energy released is accumulated along the contactor length causing a temperature rise. The radial temperature gradient is almost negligible due to the excellent heat transfer within and between the domains. A variation of temperature can be observed along the fiber length. Temperature reaches a maximum value of 317, 310, 312 and 325 K for ILs $[N_{1111}][Gly]$, $[C_2mim][Gly]$, $[C_4mim][Gly]$ and $[C_6mim][Gly]$, respectively. A high magnitude of temperature gradient can be observed in the lateral section of the fiber.

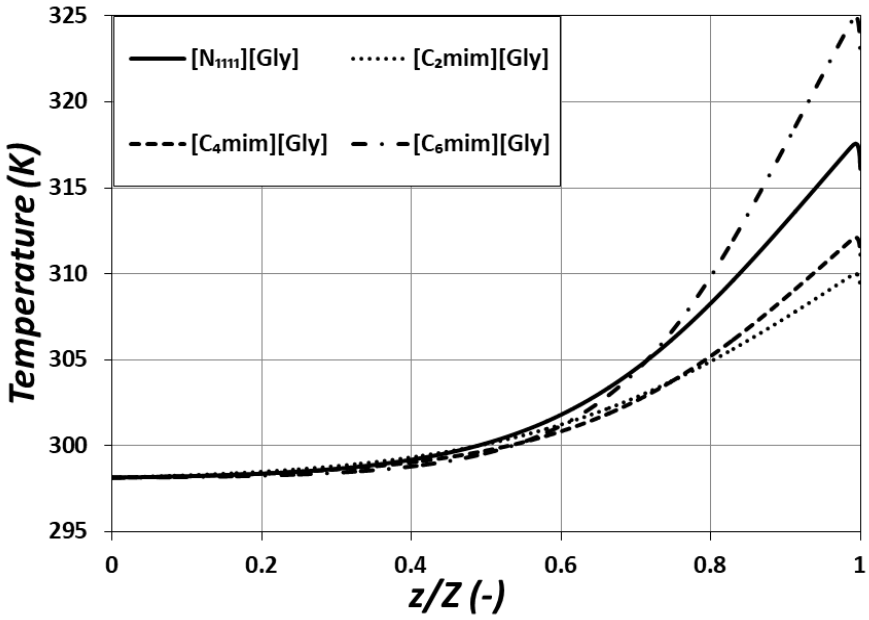

Figure 7 Temperature profile of the liquid phase over mass transfer interface; $Q_{IL} = 20\ ml\ min^{-1}$, $Q_g = 60\ ml\ min^{-1}$, $C_{i,l-in} = 0\ mol\ L^{-1}$, $C_{IL-in} = 1\ mol\ L^{-1}$, $T_{l-in}, T_{g-in} = 298\ K$

The reaction rate constant (K_2) is a function of temperature. K_2 values and their dependency upon temperature are listed in Table 2. These values were recorded near the interfacial boundary at the inlet temperature of 298 K. There is a gradual evolution of K_2 along the fiber

length as K_2 is a function of temperature, which is presented in Figure 8. In order to understand and observe the trend and compare the values between different ILs, the K_2 values were normalized by the maximum value at the corresponding axial boundary. Correspondence in the trends (Figures 6 and 7) of K_2 and temperature variation along fiber length can be evidently observed. K_2 for the IL [C₆mim][Gly] seems to have a strong dependency on temperature compared to the other three ILs. A very slight change in the K_2 can be observed for IL [C_2mim][Gly].

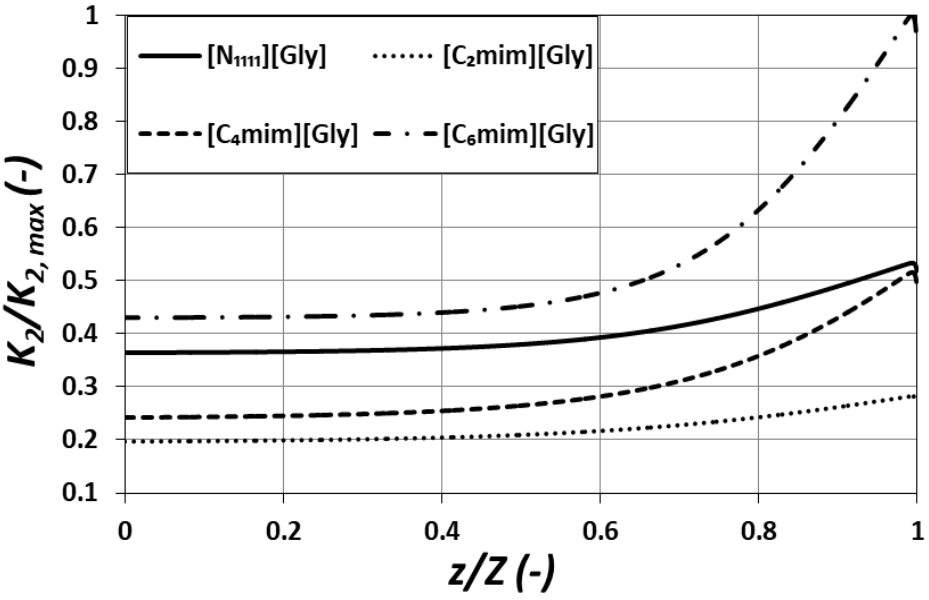

Figure 8 Normalized axial reaction rate constant distribution over mass transfer interface; $Q_{IL} = 20\ ml\ min^{-1}$, $Q_g = 60\ ml\ min^{-1}$, $C_{i,l-in} = 0\ mol\ L^{-1}$, $C_{IL-in} = 1\ mol\ L^{-1}$, $T_{l-in}, T_{g-in} = 298\ K$

4.3 ILs performance

Separation performances of the ILs were evaluated by comparing the radial profiles of the normalized gas-phase CO_2 concentration and separation efficiency at the specified axial length. Separation efficiency was calculated from the following equation.

$$Separation\ effcicinecy = \left(1 - \frac{C_{i,g}}{C_{i,g-in}}\right) \times 100 \quad (27)$$

Simulations of the gas phase CO_2 concentrations were obtained at 298 K inlet temperature for the relative radial length of the shell (r/r_s). The effect of the IL concentration (C_{IL}) and process temperature on separation performance was evaluated and reported in Figures 7 and 8, respectively.

The concentration of IL has a strong influence on the separation performance of the four ILs. On one hand, an increase in IL concentration decreases both diffusivity and solubility of CO_2 in the aqueous solution of IL, on the other hand, it increases the reaction rate [46,69]. The decrease in solubility is in accord with the salting out effect [61]. Diffusivity and physical solubility are very important parameters which strongly influence the CO_2 separation in membrane contactors. A decrease in both parameters decreases the separation efficiency. The overall effect can be observed in Figure 9, which shows that generally the efficiency is enhanced by an increase in IL concentration. This confirms the stronger influence of reaction rate as an increase in IL concentration decreases diffusivity and solubility of CO_2 and increases the reaction rate. The lower CO_2 concentration (Figure 7) represents higher separation performance. For IL $[N_{1111}][Gly]$ the efficiency increases by 23 % for increasing IL concentration from 0.3 to 2.0 mol L^{-1}. For $[C_2mim][Gly]$ an efficiency increase of 18 % was observed for increasing IL concentration 0.5 to 1.5 mol L^{-1}. Further increase in IL concentration has decreased efficiency. This phenomenon can be linked with the strong dependence of the membrane contactor absorption process on the physicochemical (viscosity, density and diffusion coefficient) properties of the absorbent. Similarly, for $[C_4mim][Gly]$ an efficiency increase of 18 % was observed for increasing IL concentration from 0.5 to 2.0 mol L^{-1} while for $[C_6mim][Gly]$ the increase was 13 % for an increase in IL concentration from 0.5 to 1.2 mol L^{-1}.

A comparative analysis of the performance of four ILs was carried out at IL concentration of 1 mol L^{-1}. ILs $[N_{1111}][Gly]$, $[C_2mim][Gly]$, $[C_4mim][Gly]$ and $[C_6mim][Gly]$ have diffusivities

of 1.06 x 10^{-9} m^2 s^{-1}, 1.66 x 10^{-9} m^2 s^{-1}, 1.55 x 10^{-9} m^2 s^{-1} and 1.14 x 10^{-9} m^2 s^{-1}, respectively. Thus based on the CO_2 diffusivity, these ILs can be ranked as, [C_2mim][Gly] > [C_4mim][Gly] > [C_6mim][Gly] > [N_{1111}][Gly]. ILs [N_{1111}][Gly], [C_2mim][Gly], [C_4mim][Gly] and [C_6mim][Gly] have physical solubilities of 2.63 x 10^{-4} mol m^{-3} Pa^{-1}, 2.52 x 10^{-4} mol m^{-3} Pa^{-1}, 2.48 x 10^{-4} mol m^{-3} Pa^{-1} and 2.7 x 10^{-4} mol m^{-3} Pa^{-1}, respectively. Thus based on the CO_2 solubility, these ILs can be ranked as, [C_6mim][Gly] > [N_{1111}][Gly] > [C_2mim][Gly] > [C_4mim][Gly]. Based on the K_2 values from Table 2, ILs can be ranked as [C_6mim][Gly] > [N_{1111}][Gly] > [C_4mim][Gly] > [C_2mim][Gly]. Based on the overall performance at IL concentration of 1 mol L^{-1}, the four ILs can be ranked as [C_6mim][Gly] > [C_2mim][Gly] > [C_4mim][Gly] > [N_{1111}][Gly]. IL [C_6mim][Gly] was found with the highest efficiency of 85 % among all ILs. While comparing the ILs at 2 mol L^{-1} the efficiencies were 83, 75 and 75 % for [C_4mim][Gly], [C_2mim][Gly] and [N_{1111}][Gly], respectively. Thus, it can be concluded that the overall separation performance is the combined effect of all three parameters, diffusivity, solubility and reaction rate. An increase in the CO_2 solubilities has been reported with an increase in the alkyl chain of the imidazolium cation [70,71]. However, the effect of the alkyl chain cation was found to be minor compared to anions [72]. This effect seems to be validated in regard to the separation efficiencies of imidazolium cation based ILs reported above.

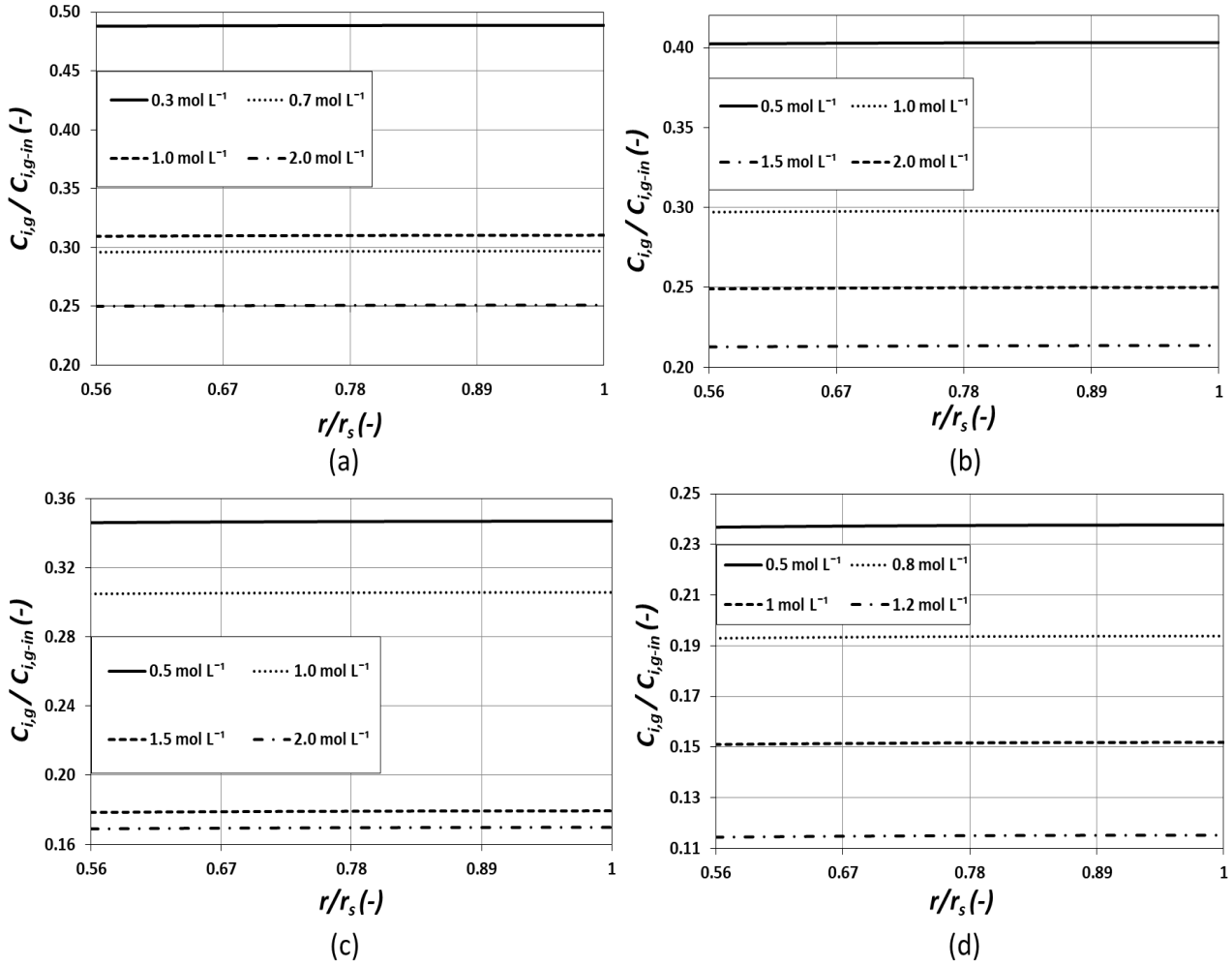

Figure 9 Normalized radial profiles of gas-phase CO_2 concentrations for different concentration of ionic liquids (a) $[N_{1111}][Gly]$, (b) $[C_2mim][Gly]$, (c) $[C_4mim][Gly]$ and (d) $[C_6mim][Gly]$; $Q_{IL} = 20\ ml\ min^{-1}$, $Q_g = 60\ ml\ min^{-1}$, $C_{i,l-in} = 0\ mol\ L^{-1}$, $T_{l-in}, T_{g-in} = 303\ K$

Temperature can affect both physisorption and chemisorption of the CO_2 in ILs. Normally, in the case of the absorption process with a chemical reaction, the temperature can affect the physical solubility, diffusivity, and reaction rate. Physical solubility of CO_2 in the ILs decreases with an increase in temperature [20,73]. Diffusivity of the CO_2 in ILs and gaseous mixture has proportionality with the temperature. An increase in temperature increases the diffusivity of CO_2 due to a decrease in the viscosity of the ILs. Similar results have been reported in other literature [51,59]. Feng et al. [46] reported that an increase in temperature increases the reaction rate of the glycine based ILs. The overall effect of temperature on the

absorption performance can be observed in Figure 10. An increase can be observed in the separation performance with an increase in temperature. However, the increase is less compared to that observed for IL concentration. An increase in temperature from 298 to 323 K has increased the efficiency by nearly 1, 3, 11 and 5 % for ILs $[N_{1111}][Gly]$, $[C_2mim][Gly]$, $[C_4mim][Gly]$ and $[C_6mim][Gly]$, respectively. Effect of temperature on the separation performance of IL $[N_{1111}][Gly]$ was almost negligible. Strong influence of temperature can be observed for IL $[C_4mim][Gly]$.

The enhancement in the separation efficiency with an increase in IL concentration (higher reaction rates) and temperature (higher reaction rates and diffusivities) also shows the dominance of the chemisorption over the physisorption in the current membrane contactor absorption process. It is noteworthy here that the process was steady-state and the IL entering the contactor was always unloaded.

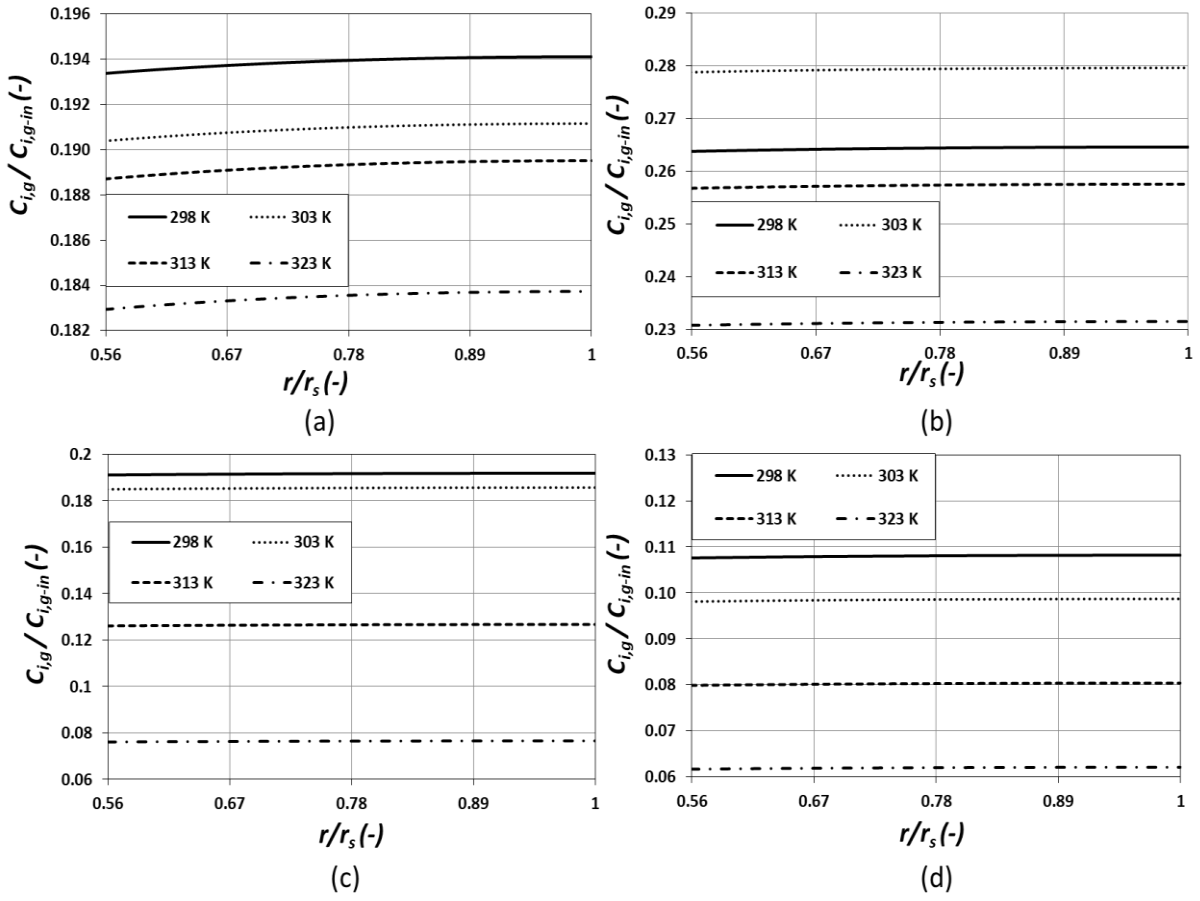

Figure 10 Normalized radial profiles of gas phase CO_2 concentrations at different process temperatures for ionic liquids (a) $[N_{1111}][Gly]$, (b) $[C_2mim][Gly]$, (c) $[C_4mim][Gly]$ and (d) $[C_6mim][Gly]$; $Q_{IL} = 20\ ml\ min^{-1}$, $Q_g = 60\ ml\ min^{-1}$, $C_{i,l-in} = 0\ mol\ L^{-1}$, $C_{IL-in} = 1\ mol\ L^{-1}$

4.4 Boundary flux across the gas/liquid interface

Figure 11 shows the local boundary flux of the CO_2 across the mass transfer interface for the four ILs at different concentrations. For all ILs, the local flux profiles pass through a maximum value near the fiber length of z/Z=1. The local CO_2 flux increases with a slow rate starting from z/Z=0. However, the rate increases as the profile moves toward the fiber length of z/Z=1. The effect of IL concentration on the CO_2 boundary flux is very evident from Figure 10. The trend of the boundary flux can be divided into two parts, before half contactor length, and after half contactor length. Near the CO_2 inlet boundary (z/Z=1) boundary flux is higher for high IL concentration, which decreases with the contactor length. The effect of IL concentration is almost negligible near the half contactor length. Moving toward the CO_2 exit boundary (z/Z=0) from the half contactor length the boundary flux of the lower IL concentration becomes dominant. Due to the high concentration of CO_2 near the inlet, there is a high driving force which leads to high values of flux. The CO_2 concentration is very low in the section before the half contactor length due to the high absorption near the inlet. Therefore there is a low driving force and low flux. Among all of the IL $[C_6mim][Gly]$ has shown the highest boundary flux. As the high IL concentration means low diffusivity and low solubility, yet again the dominance of chemisorption over physisorption was observed for the current absorption process.

The average flux for ILs of this study were nearly 1 magnitude higher than those reported by Lu et al. [74] for TSIL 1-(3-aminopropyl)-3-methyl-imidazolium tetrafluoroborate

([apmim][BF_4]). The average simulated CO_2 flux for the four ILs of this study was in the range of 2.1-2.3 (x 10^{-3} mol m^2 s^{-1}) while the maximum flux reported by Lu et al. for IL [apmim][BF_4], was 6 x 10^{-4} mol m^2 s^{-1}. In another study, Lu et al. [75] developed IL diethanolamine glycinate for CO_2 capture. The study has reported a membrane flux of 6.6 x 10^{-4} mol m^2 s^{-1}.

The effect of temperature on the boundary flux is presented in Figure 12. For ILs [N_{1111}][Gly] and [C_2mim][Gly], the effect of temperature on the CO_2 boundary flux is nearly negligible. In case of ILs [C_4mim][Gly] and [C_6mim][Gly], the boundary flux of CO_2 is affected by change in temperature. Stronger influence of the temperature on the CO_2 boundary flux can be observed for IL [C_4mim][Gly]. Similar effects were observed for the temperature influence on the separation efficiency and were reported in Section 3.2. For all ILs, the boundary flux profiles pass through a maximum value near the fiber length of z/Z=1. For ILs [C_4mim][Gly] and [C_6mim][Gly], the CO_2 boundary flux trend can be divided in two parts, before half contactor length and after half contactor length. Near the CO_2 inlet boundary (z/Z=1) boundary flux is higher for high temperatures, which decreases with the contactor length. The effect of temperature is almost negligible near the contactor length z/Z=0.7. Moving toward the CO_2 exit boundary (z/Z=0) from the half contactor length the boundary flux at lower temperatures becomes dominant.

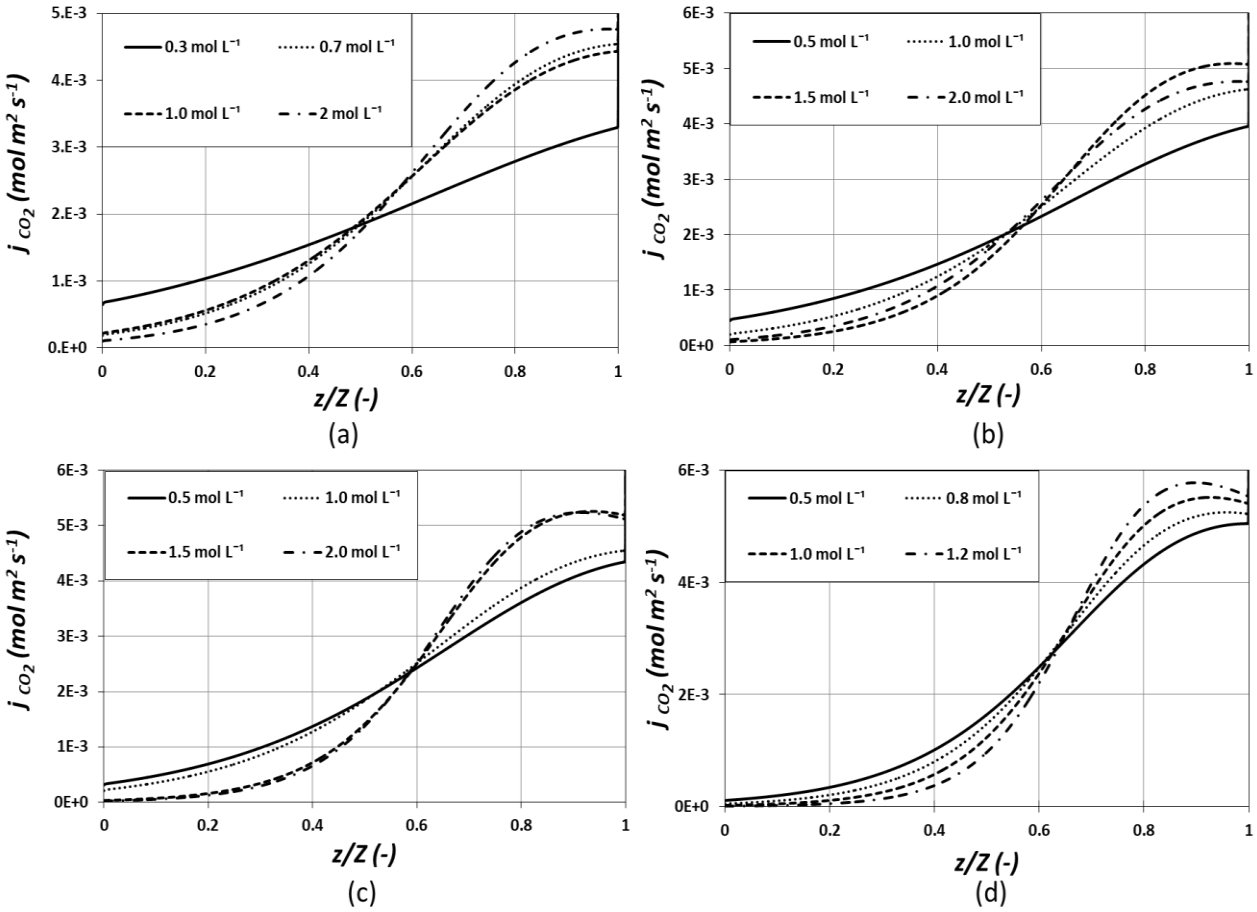

Figure 11 Axial profiles of the CO_2 boundary flux across the mass transfer interface for different concentrations of the ionic liquids (a) $[N_{1111}]$[Gly], (b) $[C_2mim]$[Gly], (c) $[C_4mim]$[Gly] and (d) $[C_6mim]$[Gly]; $Q_{IL} = 20\ ml\ min^{-1}$, $Q_g = 60\ ml\ min^{-1}$, $C_{i,l-in} = 0\ mol\ L^{-1}$, $T_{l-in}, T_{g-in} = 303\ K$

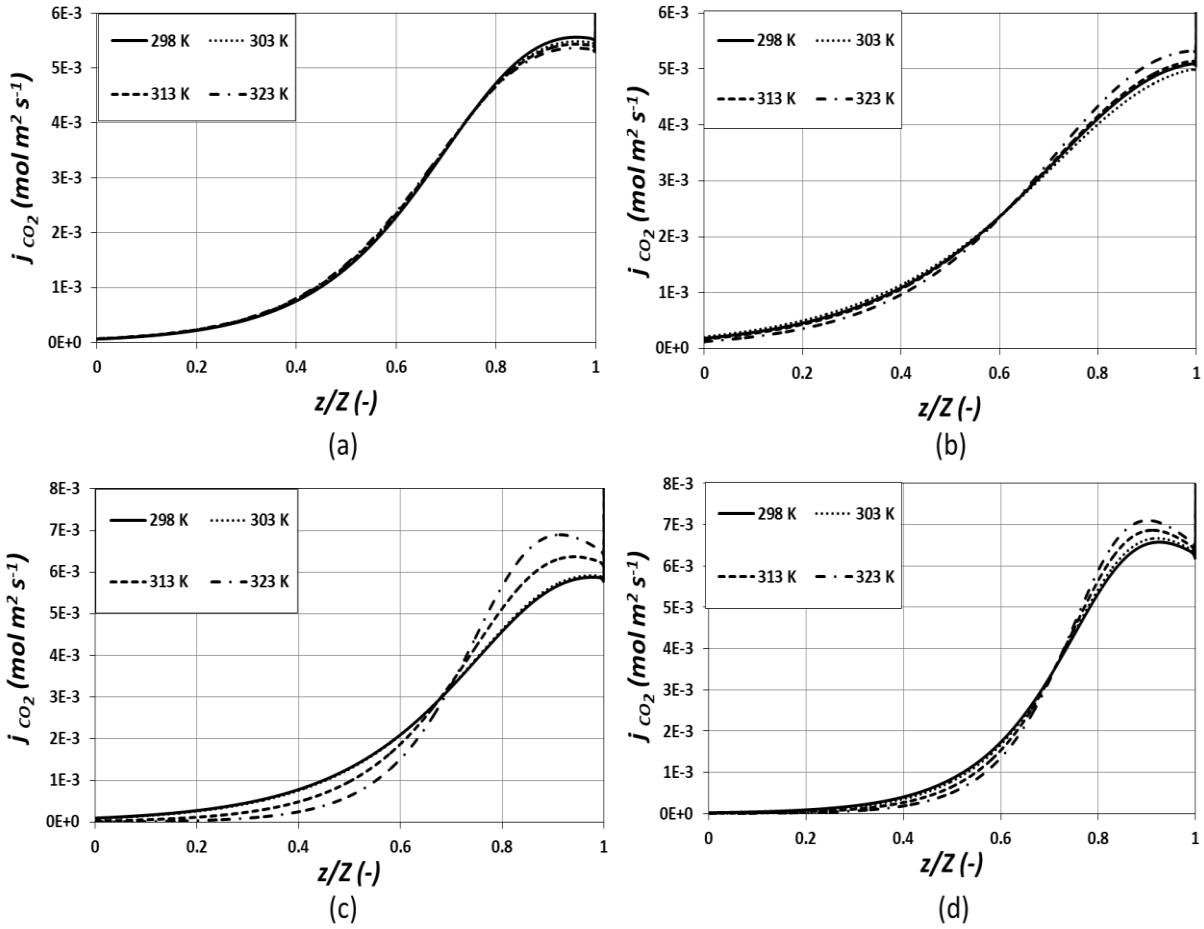

Figure 12 Axial profiles of the CO_2 boundary flux across the mass transfer interface at different process temperatures for the ionic liquids (a) [N_{1111}][Gly], (b) [C_2mim][Gly], (c) [C_4mim][Gly] and (d) [C_6mim][Gly]; $Q_{IL} = 20\ ml\ min^{-1}$, $Q_g = 60\ ml\ min^{-1}$, $C_{i,l-in} = 0\ mol\ L^{-1}$, $C_{IL-in} = 1\ mol\ L^{-1}$

4.5 Reaction rate across the gas/liquid interface

Axial profiles of the reaction rate of CO_2 for the four ILs are presented in Figure 13. As discussed in the preceding sections, due to the high values of Hatta number, dominancy of chemisorption over physisorption and consideration of unloaded solvent at the inlet the absorption can be considered to happen mostly near the interface. Thus the axial profile of the reaction rate presented here was calculated over the interfacial boundary. In order to observe the trend, these values were normalized with the maximal value over the corresponding axial length. The very strong influence of the IL concentration on the reaction rate can be observed.

Starting near the contactor length of z/Z=0, the reaction rate is a little higher for low IL concentrations than that of high IL concentrations. Moving along the contactor length the reaction rate becomes very high for the high IL concentrations. The low reaction rates for the high ILs concentration near the liquid inlet (z/Z=0) are due to the very low concentration of CO_2 at the gas outlet (z/Z=0). In the case of high IL concentrations, the CO_2 is absorbed very quickly at the gas side inlet (z/Z=1). The maximal values of the reaction rate for all ILs were recorded near the contactor length at z/Z=0.8. The reaction rate is maximum near this point due to the availability of optimal reactants concentration, as can be seen from Figure 6. Also, the reaction rate is affected by rate constant, which increases along contactor length with increase in temperature and reaches a maximum near that point. Hoff et al. [76] and Hoff and Svendsen [77] reported that the complex formation after the reaction affects the overall absorption process. However, due to unloaded solvent and steady-state conditions, the reaction mostly occurs near the interface and the effect can be neglected on the overall absorption. Moreover, very high liquid flowrates were used in their studies, which create radial concentration gradients.

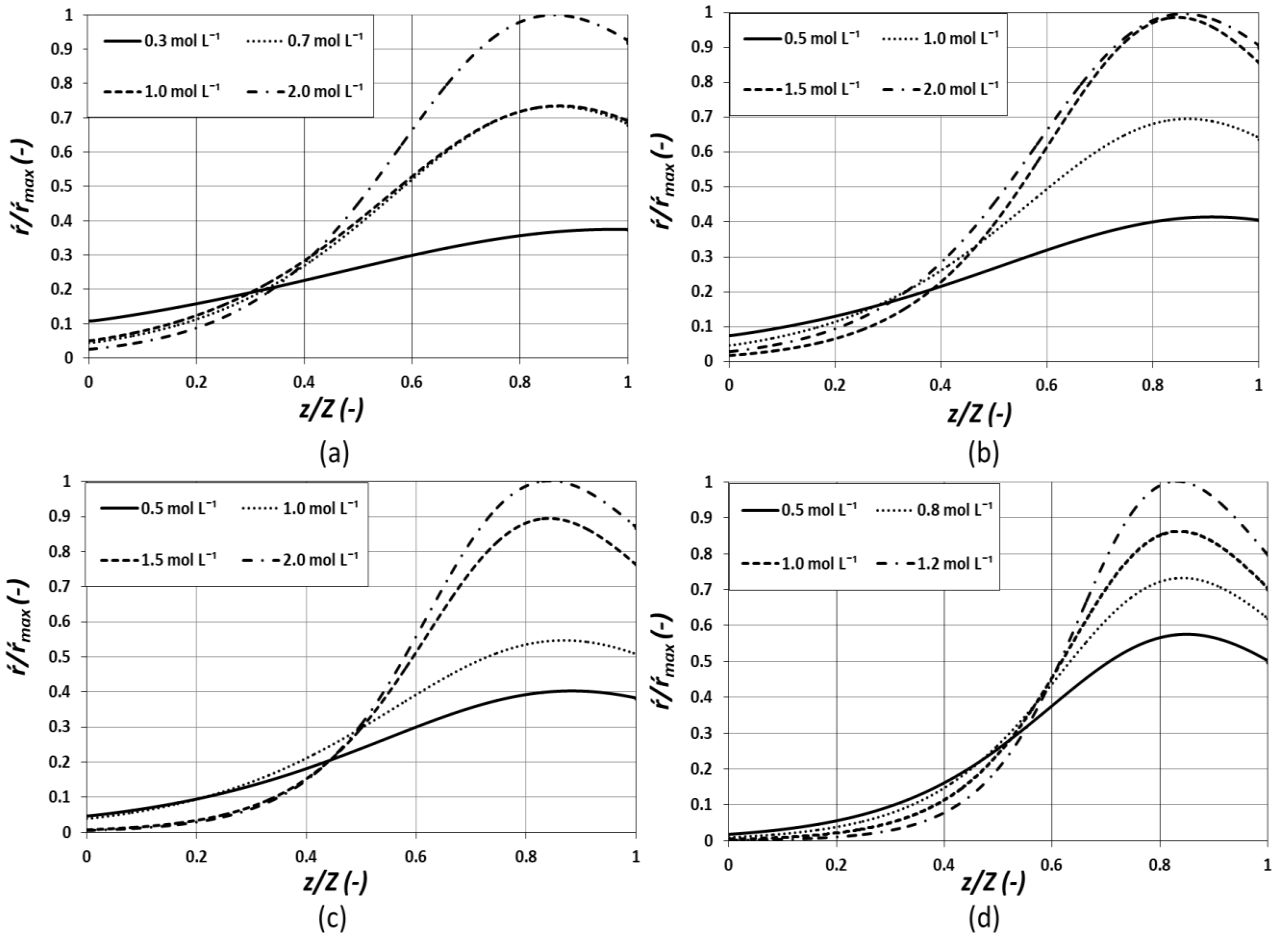

Figure 13 Axial profiles of the reaction rate across the mass transfer interface for different concentrations of the ionic liquids (a) [N_{1111}][Gly], (b) [C_2mim][Gly], (c) [C_4mim][Gly] and (d) [C_6mim][Gly]; $Q_{IL} = 20\ ml\ min^{-1}$, $Q_g = 60\ ml\ min^{-1}$, $C_{i,l-in} = 0\ mol\ L^{-1}$, $T_{l-in}, T_{g-in} = 303\ K$

Variation of the reaction rate along with the fiber length cannot only be justified by the variation in the CO_2 and IL concentrations. It can be seen from Figure 7 of the temperature profile that there is a gradual increase in the temperature along the fiber length which affects the reaction rate along the fiber. It can also be observed from Figure 8 of the reaction rate constant with gradually increases along the fiber length. The overall effect of temperature on the reaction rate is presented in Figure 14. The effect is lower compared to that reported for IL concentration. On the overall, the reaction rate is enhanced with high temperatures. The

reaction rate of the IL [C_4mim][Gly] seems to be highly affected with temperature while the effect is very low for IL [N_{1111}][Gly].

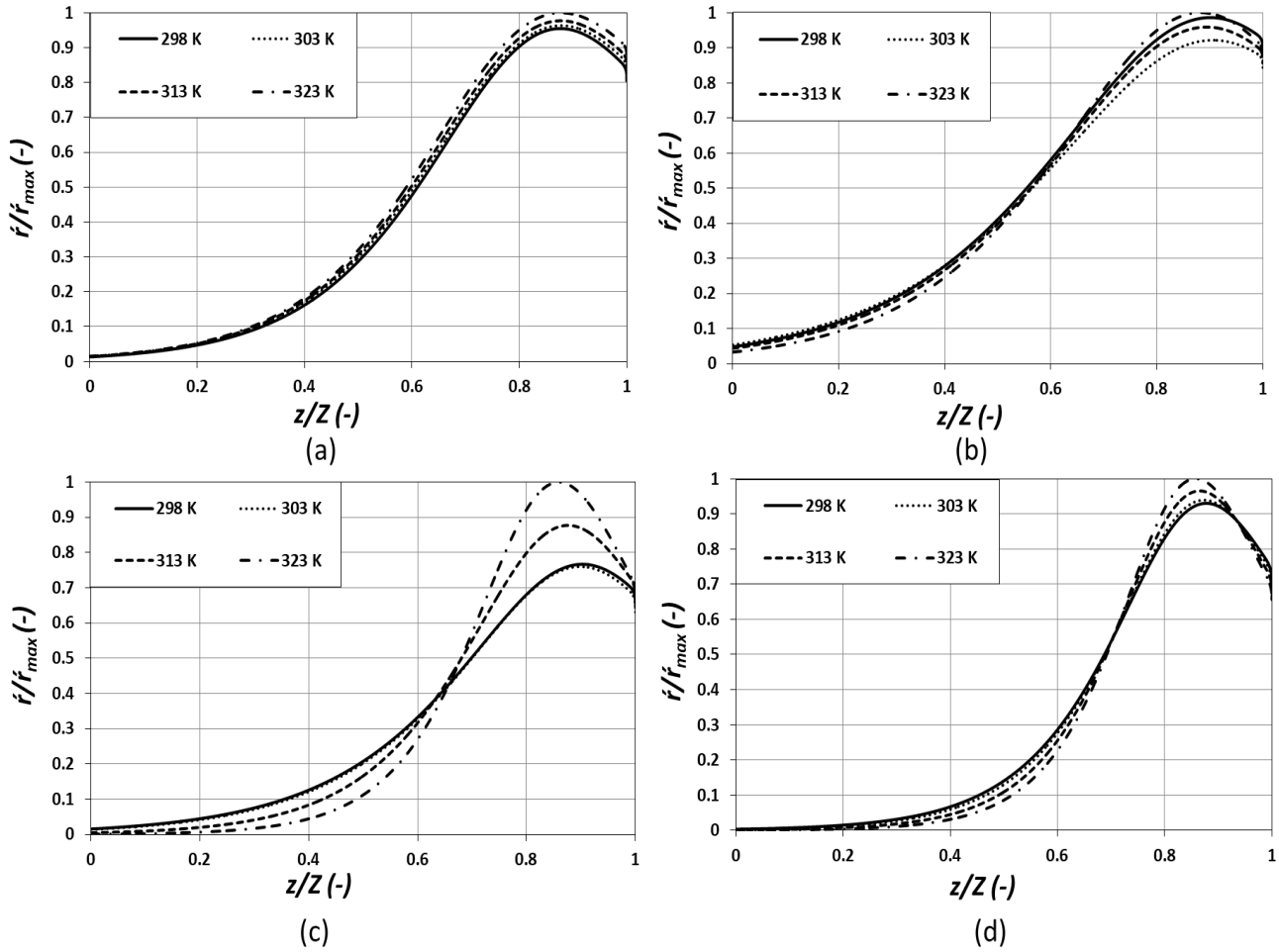

Figure 14 Axial profiles of the reaction rate across the mass transfer interface at different process temperatures for the ionic liquids (a) [N_{1111}][Gly], (b) [C_2mim][Gly], (c) [C_4mim][Gly] and (d) [C_6mim][Gly]; $Q_{IL} = 20\ ml\ min^{-1}$, $Q_g = 60\ ml\ min^{-1}$, $C_{i,l-in} = 0\ mol\ L^{-1}$, $C_{IL-in} = 1\ mol\ L^{-1}$

5 Conclusion

The aim of this work was to develop a non-isothermal mass and energy transport model for the chemisorption and physisorption of CO_2 into the highly reactive amino acid-based ILs

used as absorbents in the membrane contactor. The ILs considered for this study have never been reported in the literature for membrane-based CO_2 absorption operations. The non-isothermal modeling approach implemented here for the reactive amino acid-based ILs is a new approach to study the axial temperature and its dependent parameter variations in the membrane contactor due to the dissolution reaction. The model adopts steady-state conditions by considering open-loop flow for unloaded absorbents and gas mixtures. Detailed analyses of the concentration, temperature, and rate constant profiles were performed. Notable temperature variations along the length of the contactor were recorded which further influenced the other dependent parameters, including diffusivity solubility, rate constant and reaction rate. ILs concentration showed a strong influence on the CO_2 separation performance of ILs, CO_2 boundary flux and reaction kinetics between CO_2 and ILs, rather than process temperature. Considering IL concentration of 1 mol L^{-1}, based on the diffusivity, solubility, rate constant and overall separation performance, the four ILs can be ranked as [C_2mim][Gly] > [C_4mim][Gly] > [C_6mim][Gly] > [N_{1111}][Gly], [C_6mim][Gly] > [N_{1111}][Gly] > [C_2mim][Gly] > [C_4mim][Gly], [C_6mim][Gly] > [N_{1111}][Gly] > [C_4mim][Gly] > [C_2mim][Gly] and [C_6mim][Gly] > [C_2mim][Gly] > [C_4mim][Gly] > [N_{1111}][Gly], respectively. The overall separation performance is the result of the combined effect of these three parameters. No evident variations were found in the radial heat transfer profiles. The mass transfer was effective near the interface due to the presence of very reactive absorbents and the chemisorption was predominant. The influence of the diffusion of reaction products on overall absorption was neglected as the reaction was dominant only over and/or near the interface. A comparison between experimental data and simulation was carried out which confirmed the similar trend between the simulations and experimental data and hence validate the model. Considering the facts presented in this work, the absorbent used here are appropriate solvents for CO_2 capture. Additional experimental investigations and modeling

work are needed to extend this study for severe industrial operating conditions and to make it a feasible technology.

Nomenclature

C	Concentration (mol m^{-3})
C_p	Specific heat (J mol^{-1} K^{-1})
D	Diffusivity (m^2 s^{-1})
E	Enhancement factor (-)
H	Solubility of CO_2 (mol m^{-3} Pa^{-1})
H*	Henry's law constant (atm)
H_a	Hatta number (-)
ΔH_{abs}	Enthalpy (J mol^{-1})
j	Mass transfer flux (mol m^2 s^{-1})
K_2	2^{nd} order rate constant (L mol^{-1} s^{-1})
K_{ov}	Overall kinetic constant (s^{-1})
K_l	Liquid film mass transfer coefficient (m s^{-1})
m	Distribution coefficient of CO_2 (-)
M	Molar weight (Kg mol^{-1})
N	Number of fibers
P	Pressure (Pa)
Q	Volumetric flowrate (m^3 s^{-1})
r	Radial coordinate (m)
r_i	Inner radius of the tube (m)
r_e	Outer radius of the tube (m)
r_s	Radius of the free surface (m)
r_c	Module inner radius (m)
ŕ	Reaction rate (mol m^{-3} s^{-1})
R	Perfect gas constant (J mol^{-1} K^{-1})

Subscripts

t	Time (s)
T	Temperature (K)
u	Average velocity (m s^{-1})
U	Velocity (m s^{-1})
v	Molar volume (cm^3 mol^{-1})
V	Volume (m^3)
Z	Effective membrane length (m)
z	Axial coordinate (m)
g	Gas
i	Component/specie
IL	Ionic Liquid
in	Inlet
l	Liquid
ov	Overall
r	Radial
Z	Axial

Greek Letters

μ	Viscosity (cP)
∅	Volumetric void fraction (-)
ρ	Density (Kg m^{-3})
ε	Porosity of the membrane (-)
τ	Tortuosity of the membrane (-)
δ	Thickness of the membrane (m)
λ	Thermal conductivity (W m^{-1} K^{-1})

References

[1] M. Wang, A. Lawal, P. Stephenson, J. Sidders, C. Ramshaw, Post-combustion CO2 capture with chemical absorption: A state-of-the-art review, Chem. Eng. Res. Des. (2011). https://doi.org/10.1016/j.cherd.2010.11.005.

[2] K.M.K. Yu, I. Curcic, J. Gabriel, S.C.E. Tsang, Recent advances in CO2 capture and utilization., ChemSusChem. (2008). https://doi.org/10.1002/cssc.200800169.

[3] S. Zhao, P.H.M. Feron, L. Deng, E. Favre, E. Chabanon, S. Yan, J. Hou, V. Chen, H. Qi, Status and progress of membrane contactors in post-combustion carbon capture: A state-of-the-art review of new developments, J. Memb. Sci. 511 (2016) 180–206. https://doi.org/10.1016/j.memsci.2016.03.051.

[4] Q. Sohaib, J.M. Vadillo, L. Gómez-Coma, J. Albo, S. Druon-Bocquet, A. Irabien, J. Sanchez-Marcano, Post-combustion CO2 capture by coupling [emim] cation based ionic liquids with a membrane contactor; Pseudo-steady-state approach, Int. J. Greenh. Gas Control. (2020). https://doi.org/10.1016/j.ijggc.2020.103076.

[5] D.M. D'Alessandro, B. Smit, J.R. Long, Carbon dioxide capture: Prospects for new materials, Angew. Chemie - Int. Ed. (2010). https://doi.org/10.1002/anie.201000431.

[6] J.D. Figueroa, T. Fout, S. Plasynski, H. McIlvried, R.D. Srivastava, Advances in CO2 capture technology-The U.S. Department of Energy's Carbon Sequestration Program, Int. J. Greenh. Gas Control. (2008). https://doi.org/10.1016/S1750-5836(07)00094-1.

[7] A.L. Kohl, R.B. Nielsen, Gas purification 5th ed, Houst. Gulf Publ. Co. (1997). https://doi.org/10.1016/B978-088415220-0/50009-4.

[8] M. Aghaie, N. Rezaei, S. Zendehboudi, A systematic review on CO 2 capture with ionic liquids: Current status and future prospects, Renew. Sustain. Energy Rev. (2018). https://doi.org/10.1016/j.rser.2018.07.004.

[9] C.H. Yu, C.H. Huang, C.S. Tan, A review of CO2 capture by absorption and adsorption, Aerosol Air Qual. Res. (2012). https://doi.org/10.4209/aaqr.2012.05.0132.

[10] F.F. Chen, K. Huang, J.P. Fan, D.J. Tao, Chemical solvent in chemical solvent: A class of hybrid materials for effective capture of CO2, AIChE J. (2018). https://doi.org/10.1002/aic.15952.

[11] Q. Sohaib, J.M. Vadillo, L. Gómez-Coma, J. Albo, S. Druon-Bocquet, A. Irabien, J. Sanchez-Marcano, CO2 capture with room temperature ionic liquids; coupled absorption/desorption and single module absorption in membrane contactor, Chem. Eng. Sci. (2020). https://doi.org/10.1016/j.ces.2020.115719.

[12] N. MacDowell, N. Florin, A. Buchard, J. Hallett, A. Galindo, G. Jackson, C.S. Adjiman, C.K. Williams, N. Shah, P. Fennell, An overview of CO2 capture technologies, Energy Environ. Sci. (2010). https://doi.org/10.1039/c004106h.

[13] X. Zhang, X. Zhang, H. Dong, Z. Zhao, S. Zhang, Y. Huang, Carbon capture with ionic liquids: overview and progress, Energy Environ. Sci. 5 (2012) 6668. https://doi.org/10.1039/c2ee21152a.

[14] F. Liu, K. Huang, L. Jiang, Promoted adsorption of CO2 on amine-impregnated adsorbents by functionalized ionic liquids, AIChE J. (2018). https://doi.org/10.1002/aic.16333.

[15] K. Ghandi, A Review of Ionic Liquids, Their Limits and Applications, Green Sustain. Chem. (2014). https://doi.org/10.4236/gsc.2014.41008.

[16] X. Yan, S. Anguille, M. Bendahan, P. Moulin, Ionic liquids combined with membrane separation processes: A review, Sep. Purif. Technol. (2019). https://doi.org/10.1016/j.seppur.2019.03.103.

[17] X.L. Papatryfon, N.S. Heliopoulos, I.S. Molchan, L.F. Zubeir, N.D. Bezemer, M.K. Arfanis, A.G. Kontos, V. Likodimos, B. Iliev, G.E. Romanos, P. Falaras, K. Stamatakis, K.G. Beltsios, M.C. Kroon, G.E. Thompson, J. Klöckner, T.J.S. Schubert,

CO2 capture efficiency, corrosion properties, and ecotoxicity evaluation of amine solutions involving newly synthesized ionic liquids, Ind. Eng. Chem. Res. (2014). https://doi.org/10.1021/ie501897d.
[18] Z. Dai, L. Deng, Membrane absorption using ionic liquid for pre-combustion CO2 capture at elevated pressure and temperature, Int. J. Greenh. Gas Control. 54 (2016) 59–69. https://doi.org/10.1016/j.ijggc.2016.09.001.
[19] J.B. Zhang, H. Peng, Y. Liu, D.J. Tao, P. Wu, J.P. Fan, K. Huang, Highly Efficient CO2 Capture by Polyethylenimine Plus 1-Ethyl-3-Methylimidazolium Acetate Mixed Absorbents, ACS Sustain. Chem. Eng. (2019). https://doi.org/10.1021/acssuschemeng.9b00530.
[20] Z. Lei, C. Dai, B. Chen, Gas solubility in ionic liquids, Chem. Rev. 114 (2014) 1289–1326. https://doi.org/10.1021/cr300497a.
[21] Z. Dai, R.D. Noble, D.L. Gin, X. Zhang, L. Deng, Combination of ionic liquids with membrane technology: A new approach for CO2separation, J. Memb. Sci. 497 (2016) 1–20. https://doi.org/10.1016/j.memsci.2015.08.060.
[22] M.B. Shiflett, A. Yokozeki, Phase behavior of carbon dioxide in ionic liquids: [emim][acetate], [emim][trifluoroacetate], and [emim][acetate] + [emim][trifluoroacetate] mixtures, J. Chem. Eng. Data. 54 (2009) 108–114. https://doi.org/10.1021/je800701j.
[23] C. Wang, H. Luo, D.E. Jiang, H. Li, S. Dai, Carbon dioxide capture by superbase-derived protic ionic liquids, Angew. Chemie - Int. Ed. (2010). https://doi.org/10.1002/anie.201002641.
[24] H. Ohno, K. Fukumoto, Amino acid ionic liquids, Acc. Chem. Res. (2007). https://doi.org/10.1021/ar700053z.
[25] C. Wang, Y. Guo, X. Zhu, G. Cui, H. Li, S. Dai, Highly efficient CO 2 capture by tunable alkanolamine-based ionic liquids with multidentate cation coordination, Chem. Commun. (2012). https://doi.org/10.1039/c2cc32365f.
[26] S. Ren, Y. Hou, W. Wu, S. Tian, W. Liu, CO 2 capture from flue gas at high temperatures by new ionic liquids with high capacity, RSC Adv. (2012). https://doi.org/10.1039/c2ra00996j.
[27] C. Wei, G. Puxty, P. Feron, Amino acid salts for CO 2 capture at fl ue gas temperatures, Chem. Eng. Sci. 107 (2014) 218–226. https://doi.org/10.1016/j.ces.2013.11.034.
[28] H.R. Perry, Perry's Chemical Engineering Handbook, 8th Edn ed, 2007.
[29] A. Gabelman, S.-T. Hwang, Hollow fiber membrane contactors, J. Memb. Sci. 159 (1999) 61–106. https://doi.org/10.1016/S0376-7388(99)00040-X.
[30] V.Y. Dindore, D.W.F. Brilman, G.F. Versteeg, Hollow fiber membrane contactor as a gas-liquid model contactor, Chem. Eng. Sci. (2005). https://doi.org/10.1016/j.ces.2004.07.129.
[31] S. Qazi, L. Gómez-coma, J. Albo, S. Druon-bocquet, A. Irabien, CO 2 capture in a hollow fiber membrane contactor coupled with ionic liquid : Influence of membrane wetting and process parameters, Sep. Purif. Technol. 233 (2020) 115986. https://doi.org/10.1016/j.seppur.2019.115986.
[32] S. Qazi, L. Gómez-coma, J. Albo, S. Druon-bocquet, A. Irabien, Mathematical Modelling of CO 2 Absorption with Ionic Liquids in a Membrane Contactor , Study of Absorption Kinetics and Influence of Temperature, J Chem Technol Biotechnol. (2019). https://doi.org/10.1002/jctb.6265.
[33] Q. Sohaib, A. Muhammad, M. Younas, M. Rezakazemi, Modelling Pre-Combustion CO2 Capture with Tubular Membrane Contactor Using Ionic Liquids at Elevated Temperatures, Sep. Purif. Technol. (2020) 116677.

https://doi.org/10.1016/j.seppur.2020.116677.
[34] Z. Qi, E.L. Cussler, Microporous hollow fibers for gas absorption. II. Mass transfer across the membrane, J. Memb. Sci. (1985). https://doi.org/10.1016/S0376-7388(00)83150-6.
[35] D. Demontigny, P. Tontiwachwuthikul, A. Chakma, Comparing the absorption performance of packed columns and membrane contactors, Ind. Eng. Chem. Res. (2005). https://doi.org/10.1021/ie040264k.
[36] O. Falk-Pedersen, M.S. Grønvold, P. Nøkleby, F. Bjerve, H.F. Svendsen, CO 2 Capture with Membrane Contactors , Int. J. Green Energy. (2005). https://doi.org/10.1081/ge-200058965.
[37] E. Chabanon, R. Bounaceur, C. Castel, S. Rode, D. Roizard, E. Favre, Pushing the limits of intensified CO2 post-combustion capture by gas-liquid absorption through a membrane contactor, Chem. Eng. Process. Process Intensif. (2015). https://doi.org/10.1016/j.cep.2015.03.002.
[38] J.G. Lu, Z.Y. Lu, Y. Chen, J.T. Wang, L. Gao, X. Gao, Y.Q. Tang, D.G. Liu, CO<inf>2</inf> absorption into aqueous blends of ionic liquid and amine in a membrane contactor, Sep. Purif. Technol. 150 (2015) 278–285. https://doi.org/10.1016/j.seppur.2015.07.010.
[39] M. Pan, C. Wang, Ionic Liquids for Chemisorption of CO 2 , in: Mater. Carbon Capture, 2020. https://doi.org/10.1002/9781119091219.ch11.
[40] C.E. Sánchez Fuentes, D. Guzmán-Lucero, M. Torres-Rodriguez, N. V. Likhanova, J.N. Bolaños, O. Olivares-Xometl, I. V. Lijanova, CO2/N2 separation using alumina supported membranes based on new functionalized ionic liquids, Sep. Purif. Technol. (2017). https://doi.org/10.1016/j.seppur.2017.03.031.
[41] X.M. Zhang, Z.H. Tu, H. Li, L. Li, Y.T. Wu, X.B. Hu, Supported protic-ionic-liquid membranes with facilitated transport mechanism for the selective separation of CO2, J. Memb. Sci. (2017). https://doi.org/10.1016/j.memsci.2017.01.006.
[42] S. Kaviani, S. Kolahchyan, K.L. Hickenbottom, A.M. Lopez, S. Nejati, Enhanced solubility of carbon dioxide for encapsulated ionic liquids in polymeric materials, Chem. Eng. J. (2018). https://doi.org/10.1016/j.cej.2018.08.086.
[43] R. Santiago, J. Lemus, C. Moya, D. Moreno, N. Alonso-Morales, J. Palomar, Encapsulated Ionic Liquids to Enable the Practical Application of Amino Acid-Based Ionic Liquids in CO2 Capture, ACS Sustain. Chem. Eng. (2018). https://doi.org/10.1021/acssuschemeng.8b02797.
[44] G.E. Romanos, P.S. Schulz, M. Bahlmann, P. Wasserscheid, A. Sapalidis, F.K. Katsaros, C.P. Athanasekou, K. Beltsios, N.K. Kanellopoulos, CO2 capture by novel supported ionic liquid phase systems consisting of silica nanoparticles encapsulating amine-functionalized ionic liquids, J. Phys. Chem. C. (2014). https://doi.org/10.1021/jp5062946.
[45] Y.Y. Jiang, G.N. Wang, Z. Zhou, Y.T. Wu, J. Geng, Z.B. Zhang, Tetraalkylammonium amino acids as functionalized ionic liquids of low viscosity, Chem. Commun. 8 (2002) 505–507. https://doi.org/10.1039/b713648j.
[46] Z. Feng, F. Cheng-Gang, W. You-Ting, W. Yuan-Tao, L. Ai-Min, Z. Zhi-Bing, Absorption of CO2 in the aqueous solutions of functionalized ionic liquids and MDEA, Chem. Eng. J. (2010). https://doi.org/10.1016/j.cej.2010.04.013.
[47] E. Chabanon, D. Roizard, E. Favre, Modeling strategies of membrane contactors for post-combustion carbon capture: A critical comparative study, Chem. Eng. Sci. 87 (2013) 393–407. https://doi.org/10.1016/j.ces.2012.09.011.
[48] E. Chabanon, D. Roizard, E. Favre, Membrane contactors for postcombustion carbon dioxide capture: A comparative study of wetting resistance on long time scales, Ind.

Eng. Chem. Res. (2011). https://doi.org/10.1021/ie200704h.
[49] J. Albo, P. Luis, A. Irabien, Carbon dioxide capture from flue gases using a cross-flow membrane contactor and the ionic liquid 1-ethyl-3-methylimidazolium ethylsulfate, in: Ind. Eng. Chem. Res., 2010. https://doi.org/10.1021/ie1014266.
[50] Y. Gong, Z. Wang, S. Wang, Experiments and simulation of CO2 removal by mixed amines in a hollow fiber membrane module, Chem. Eng. Process. Process Intensif. (2006). https://doi.org/10.1016/j.cep.2006.01.009.
[51] G. Jing, L. Zhou, Z. Zhou, Characterization and kinetics of carbon dioxide absorption into aqueous tetramethylammonium glycinate solution, Chem. Eng. J. (2012). https://doi.org/10.1016/j.cej.2011.11.007.
[52] J. Happel, Viscous flow relative to arrays of cylinders, AIChE J. 5 (1959) 174–177. https://doi.org/10.1002/aic.690050211.
[53] P.S. Kumar, J.A. Hogendoorn, G.F. Versteeg, P.H.M. Feron, Kinetics of the reaction of CO2 with aqueous potassium salt of taurine and glycine, AIChE J. (2003). https://doi.org/10.1002/aic.690490118.
[54] Z. Wu, Y. Zhang, W. Lei, P. Yu, Y. Luo, Kinetics of CO 2 absorption into aqueous 1-ethyl-3-methylimidazolium glycinate solution, Chem. Eng. J. (2015). https://doi.org/10.1016/j.cej.2014.11.133.
[55] M. Caplow, Kinetics of Carbamate Formation and Breakdown, J. Am. Chem. Soc. (1968). https://doi.org/10.1021/ja01026a041.
[56] Danckwerts, Gas–Liquid Reactions, McGraw-Hill, New York, 1970.
[57] H. Kierzkowska-Pawlak, Determination of kinetics in gas-liquid reaction systems. An overview, Ecol. Chem. Eng. S. (2012). https://doi.org/10.2478/v10216-011-0014-y.
[58] Z. Wu, Z. Huang, Y. Zhang, Y.H. Qin, J. Ma, Y. Luo, Kinetics analysis and regeneration performance of 1-butyl-3-methylimidazolium glycinate solutions for CO 2 capture, Chem. Eng. J. (2016). https://doi.org/10.1016/j.cej.2016.03.030.
[59] H. Guo, Z. Zhou, G. Jing, Kinetics of carbon dioxide absorption into aqueous [Hmim][Gly] solution, Int. J. Greenh. Gas Control. (2013). https://doi.org/10.1016/j.ijggc.2013.03.024.
[60] A. Schumpe, The estimation of gas solubilities in salt solutions, Chem. Eng. Sci. (1993). https://doi.org/10.1016/0009-2509(93)80291-W.
[61] S. Weisenberger, A. Schumpe, Estimation of Gas Solubilities in Salt Solutions at Temperatures from 273 K to 363 K, AIChE J. (1996). https://doi.org/10.1002/aic.690420130.
[62] G.F. Versteeg, W.P.M. van Swaal, Solubility and Diffusivity of Acid Gases (CO2, N2O) in Aqueous Alkanolamine Solutions, J. Chem. Eng. Data. (1988). https://doi.org/10.1021/je00051a011.
[63] D. Camper, C. Becker, C. Koval, R. Noble, Low pressure hydrocarbon solubility in room temperature ionic liquids containing imidazolium rings interpreted using regular solution theory, Ind. Eng. Chem. Res. (2005). https://doi.org/10.1021/ie049312r.
[64] A.F.M. Barton, Handbook of Solubility Parameters and Other Cohesion Parameters, in: Handb. Solubility Parameters Other Cohes. Parameters, 1991.
[65] R. Sander, Compilation of Henry's law constants (version 4.0) for water as solvent, Atmos. Chem. Phys. 15 (2015) 4399–4981. https://doi.org/10.5194/acp-15-4399-2015.
[66] E.N. Fuller, P.D. Schettler, J.C. Giddings, A new method for prediction of binary gas-phase diffusion coefficients, Ind. Eng. Chem. 58 (1966) 18–27. https://doi.org/10.1021/ie50677a007.
[67] Barrett, Gas Absorption on a Sieve Plate, Ph.D. Thesis, University of Cambridge, 1966.
[68] J.G. Lu, H. Ge, Y. Chen, R.T. Ren, Y. Xu, Y.X. Zhao, X. Zhao, H. Qian, CO2capture

using a functional protic ionic liquid by membrane absorption, J. Energy Inst. 90 (2017) 933–940. https://doi.org/10.1016/j.joei.2016.08.001.
[69] Z. Zhou, G. Jing, L. Zhou, Characterization and absorption of carbon dioxide into aqueous solution of amino acid ionic liquid [N1111][Gly] and 2-amino-2-methyl-1-propanol, Chem. Eng. J. 204–205 (2012) 235–243. https://doi.org/10.1016/j.cej.2012.07.108.
[70] R.E. Baltus, B.H. Culbertson, S. Dai, H. Luo, D.W. DePaoli, Low-Pressure Solubility of Carbon Dioxide in Room-Temperature Ionic Liquids Measured with a Quartz Crystal Microbalance, J. Phys. Chem. B. (2004). https://doi.org/10.1021/jp036051a.
[71] Y. Chen, S. Zhang, X. Yuan, Y. Zhang, X. Zhang, W. Dai, R. Mori, Solubility of CO2 in imidazolium-based tetrafluoroborate ionic liquids, Thermochim. Acta. (2006). https://doi.org/10.1016/j.tca.2005.11.023.
[72] S. Supasitmongkol, P. Styring, High CO2 solubility in ionic liquids and a tetraalkylammonium-based poly(ionic liquid), Energy Environ. Sci. 3 (2010) 1961. https://doi.org/10.1039/c0ee00293c.
[73] O.O. Okoturo, T.J. VanderNoot, Temperature dependence of viscosity for room temperature ionic liquids, J. Electroanal. Chem. 568 (2004) 167–181. https://doi.org/10.1016/j.jelechem.2003.12.050.
[74] J.G. Lu, C.T. Lu, Y. Chen, L. Gao, X. Zhao, H. Zhang, Z.W. Xu, CO2 capture by membrane absorption coupling process: Application of ionic liquids, Appl. Energy. (2014). https://doi.org/10.1016/j.apenergy.2013.10.045.
[75] J.G. Lu, X. Li, Y.X. Zhao, H.L. Ma, L.F. Wang, X.Y. Wang, Y.F. Yu, T.Y. Shen, H. Xu, Y.T. Zhang, CO2 capture by ionic liquid membrane absorption for reduction of emissions of greenhouse gas, Environ. Chem. Lett. (2019). https://doi.org/10.1007/s10311-018-00822-4.
[76] K.A. Hoff, O. Juliussen, O. Falk-Pedersen, H.F. Svendsen, Modeling and experimental study of carbon dioxide absorption in aqueous alkanolamine solutions using a membrane contactor, Ind. Eng. Chem. Res. (2004). https://doi.org/10.1021/ie034325a.
[77] K.A. Hoff, H.F. Svendsen, Membrane contactors for CO2 absorption - Application, modeling and mass transfer effects, Chem. Eng. Sci. (2014). https://doi.org/10.1016/j.ces.2014.05.001.